NATIONAL COOPERATIVE HIGHWAY RESEARCH PROGRAM

NCHRP Report 356

Anchorage Zone Reinforcement for Post-Tensioned Concrete Girders

Transportation Research Board
National Research Council

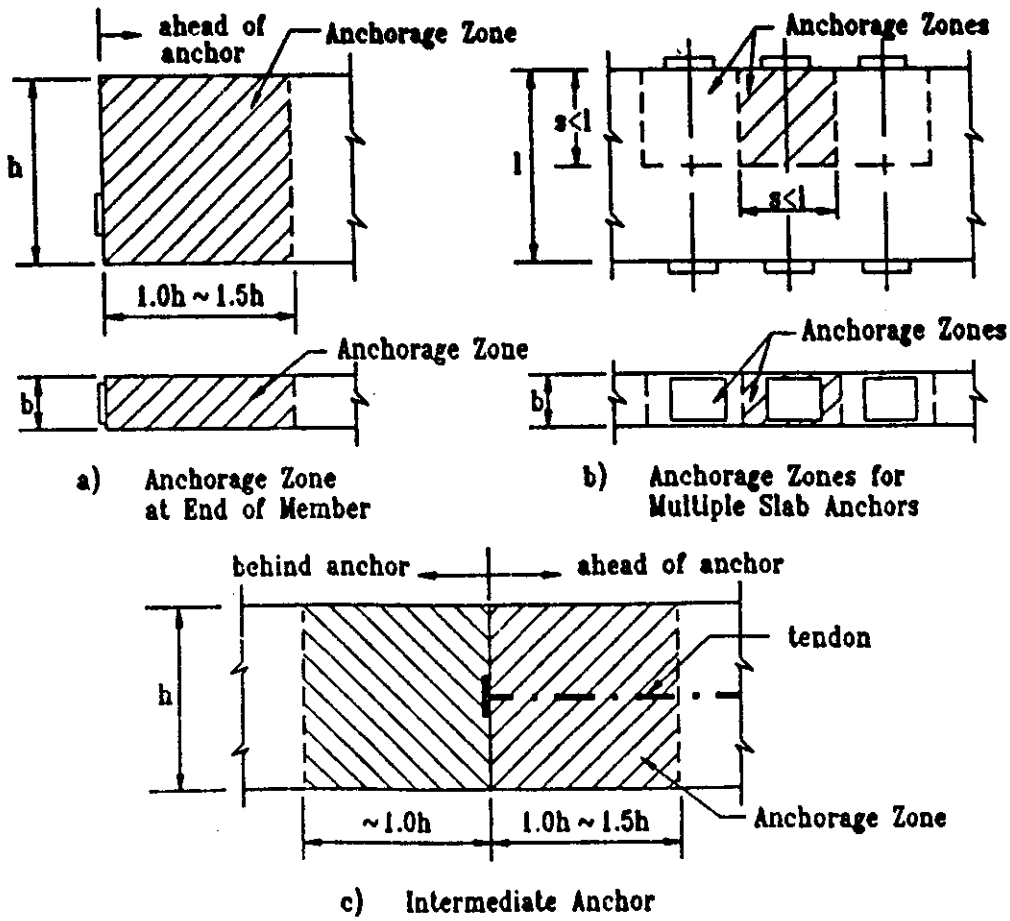

Figure 16. Anchorage zone dimensions.

of the length of the side of the anchorage device to the width of the block into which the force is transferred is one critical parameter (see Figure 18) and will be referred to as the a/h ratio. Another important ratio is the net area of the concrete supporting the plate to the net area of the bearing plate, which will be referred to as the A/A_b ratio, A is the maximum area of the portion of the supporting surface that is similar to the loaded area and concentric with it. A_g is the gross area of sufficiently rigid bearing plates (defined subsequently) or, for less rigid bearing plates, the area geometrically similar to the wedge plate with dimensions increased by twice the bearing plate thickness. A_b is the effective net area of the bearing plate calculated as the area A_g minus the area of openings in the bearing plate.

Other parameters involved in the local zone are shown in Figure 19. Edge distance is the distance from the center of the anchorage device to the nearest edge of concrete. Confinement cover is the depth of concrete over the outermost confining reinforcement, and anchor cover is the depth of concrete over the anchorage device. Spacing is the distance from the center of one anchor to the center of the next.

Parameters related to the confining steel are illustrated in Figure 20. For spiral reinforcing, the diameter of the spiral is measured from outside to outside of the steel bars, and the spiral size refers to the diameter of the reinforcing bar or rod from which the spiral is made. The pitch refers to the distance in the direction normal to the spiral diameter that is measured from the center of the bar to the center of the bar 360 deg. away. For orthogonal ties, the side length, spacing, and bar size are also illustrated in Figure 20.

In the local zone, confining reinforcing is defined as the reinforcing closely surrounding the anchorage device and providing the primary confinement. Supplementary reinforcement is reinforcing present in addition to the primary confinement reinforcing, usually added for crack control purposes (see Figure 21). Such supplementary reinforcement is often present in actual girders and is often added in anchorage device acceptance test specimens.

In order to develop a consistent design philosophy, a precise definition of the local zone is required. As illustrated in Figure 17, the local zone is defined as a rectangular prism whose transverse dimensions in each direction are: (1) when independently verified manufacturers recommendations for cover, edge distance, and spacing are not available, the larger of the plate size plus twice the minimum concrete cover required over the embedded plate for the particular application and environment, or the outer dimension of any required confining reinforcing plus the required concrete cover over the confining reinforcing steel for the particular application and environment; or (2) when independently verified manufacturers recommendations are available, the smaller

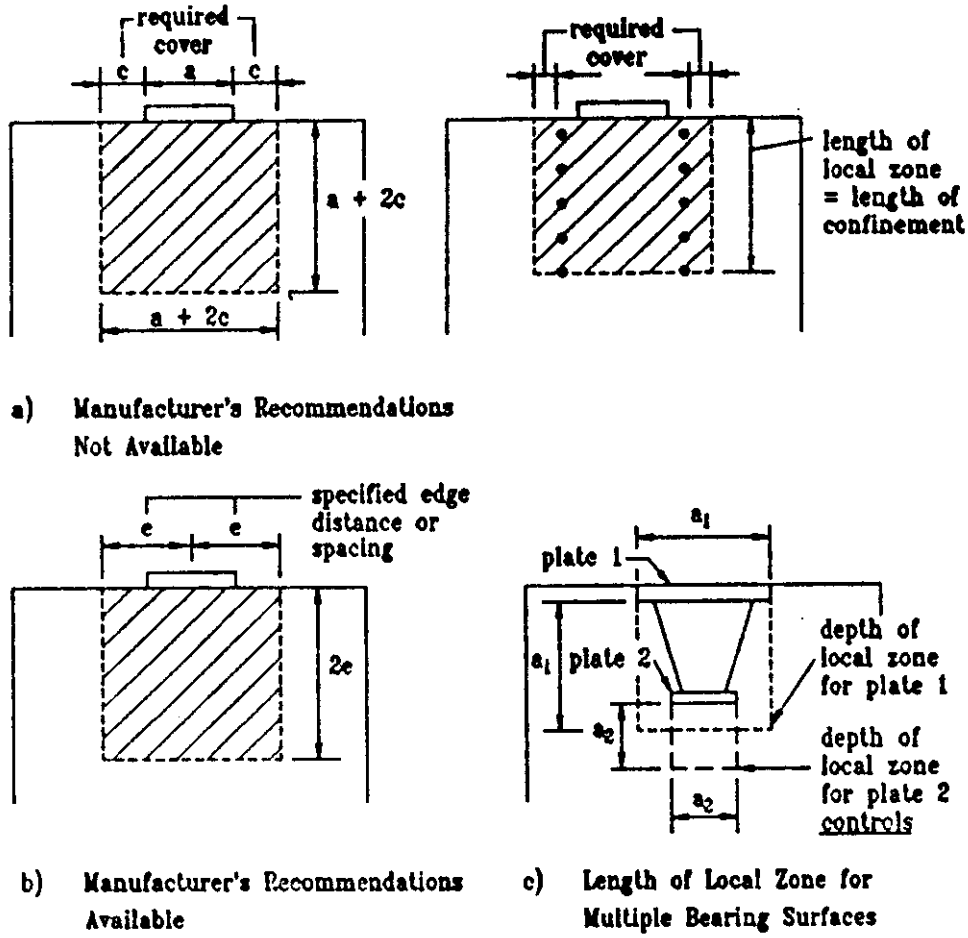

Figure 17. Local zone dimensions.

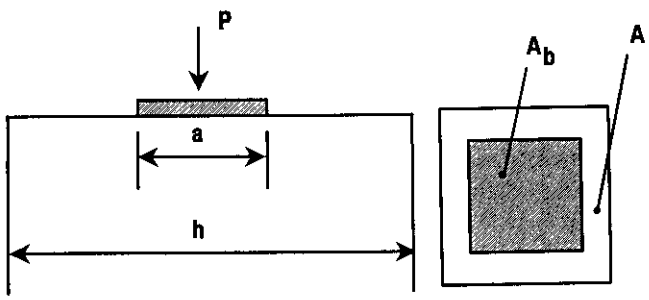

Figure 18. Definition of a/h and A/A_b ratios.

of twice the supplier's recommended edge distance, or the recommended center-to-center spacing.

The length of the local zone is defined as the greatest of the following (see Figure 17): (1) the maximum width of the local zone; (2) the length of the confining reinforcing, but no greater than 1.5 times the maximum width of the local zone; or (3) for anchorage devices with multiple bearing surfaces, distance from the loaded concrete surface to the farthest face of each bearing surface plus the maximum dimension of that bearing surface (see Figure 17c).

Rigid Bearing Plates

Based on extensive work by Hawkins (*13,14,15*), Niyogi (*35,36*), Williams (*37*), and Wurm and Daschner (*38,39*), as well as the AISC (*40*) expression for the required thickness of a bearing plate, Roberts (*4*) concluded that there were two important conditions which must be satisfied to consider a bearing plate as rigid. The first is that a flexural check indicate that the plate material does not yield. The second is that the plate be sufficiently stiff. The most complete study of the effect of stiffness of bearing plates on concrete was the work reported by Hawkins. However, all of his specimens had height to width ratios less than 1.5. Williams (*37*) and Niyogi (*35,36*) have shown that this parameter has a substantial influence and should be varied. Hawkins also used square punches (wedge plates) while most post-tensioning wedge plates are circular. Based on a reexamination of Hawkins data, Roberts found a consistent relationship between the load achieved by specimens and the calculated deflections of the edges of the plate. "Rigid" plates tended to have ratios of edge deflection to length of less than about 0.0005. Nonpublished data submitted by several post-tensioners for bearing type anchorage devices, which have been widely used without problems in the United States, indicated that ratios of edge deflection to length of about 0.00075 were actually acceptable. This can be satisfied if

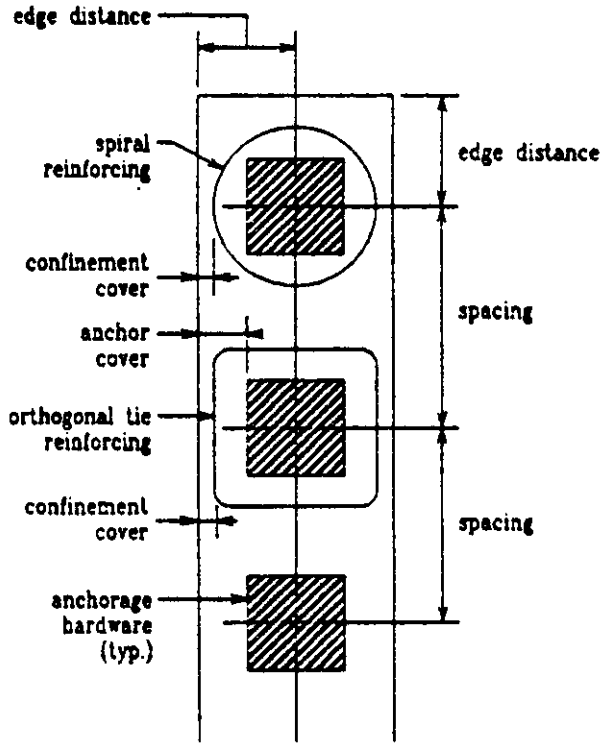

Figure 19. Parameter definitions.

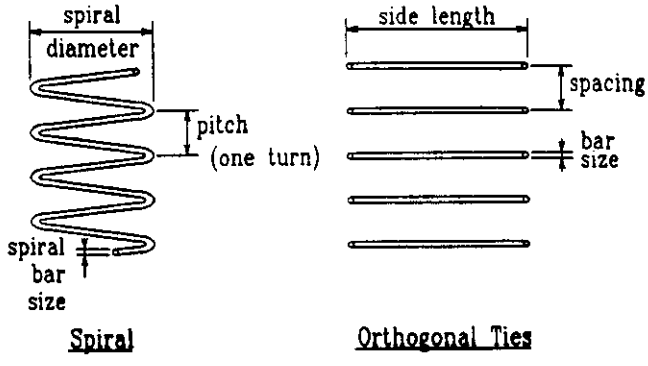

Figure 20. Confining reinforcing steel parameters.

$$n/t \geq 0.08 \sqrt[3]{E_b/f_b} \qquad (2)$$

where n is the largest distance from the outer edge of the wedge plate to the outer edge of the bearing plate, t is the average thickness of the bearing plate, E_b is the modulus of elasticity of the bearing plate material, and f_b is the maximum factored tendon load, P_u, divided by the effective bearing area A_b.

Present Code Provisions for Local Zones

In many building and bridge design standards, references to allowable or ultimate bearing stresses under post-tensioning anchorage devices are vague, conservative, and not particularly uniform. Most give formulas based on some allowable fraction of the concrete's characteristic strength and some are also a function of the A/A_b ratio.

Figure 22 indicates the wide scatter of a number of these current standards for a concentrically loaded square prism.

While most researchers have developed qualitative conclusions that agree well with one another, the quantitative conclusions are confusing, difficult to apply, and inconsistent with one another. The wide variety of bearing stresses allowed by the codes is also a source of frustration to designers. Although an increase in bearing strength due to confinement by reinforcing has been proven in many experimental programs, no code allows an increase in bearing pressure based on the amount of confining steel present. There is still much room for refinement and improvement of design guides and code provisions. In particular, specific provisions need to be included to reflect modern multiplane anchors and the effects of confining reinforcement.

Experimental Program

In this study a series of 31 test specimens were used to evaluate the behavior, test criteria, and design procedures for the local zone. Complete details are provided by Roberts (*4*). A summary of specimen details is included in Appendix C. The local zone experimental program was divided into three main categories: (1) tests to evaluate current acceptance testing procedures and develop new acceptance test procedures; (2) parametric studies; and (3) local zone-general zone interaction tests. Variables investigated included edge distance, spiral parameters, supplementary reinforcement, type of anchorage device, concrete strength, interaction with the general zone, and loading history.

Test Specimens and Methods

The majority of the specimens were very similar rectangular concrete prisms. The construction and testing procedures were almost identical. Specimen details are given in Appendix C. All specimens were cast horizontally. Tolerance on the concrete dimensions was $\pm 1/8$ in. All reinforcing steel was bent in the laboratory using CRSI standard bends and hooks. Stirrups were bent from Grade 60 deformed bars and spirals were fabricated from smooth Grade 60 bars. All reinforcing dimensions were kept within a $1/4$-in. tolerance. Strain gages were affixed to selected reinforcing bars, as shown in Figure 23. Demec locating discs for mechanical extensometer measurement of concrete surface strains were placed on two faces of every specimen as illustrated in Figure 24. All specimens were concentrically loaded through spherical heads onto wedge plates in either a 600-kip or a 1200-kip testing apparatus. The bases were uniformly supported on teflon pads. Loading was applied incrementally with careful observation of first cracking, crack development, and ultimate load. Steel strains were monitored by an automated data logger.

Tests to Evaluate Acceptance Testing Procedures—Multiple Plane Anchors

Two different recommended testing procedures were evaluated in this study. The first is the test described in the FIP *Recommen-*

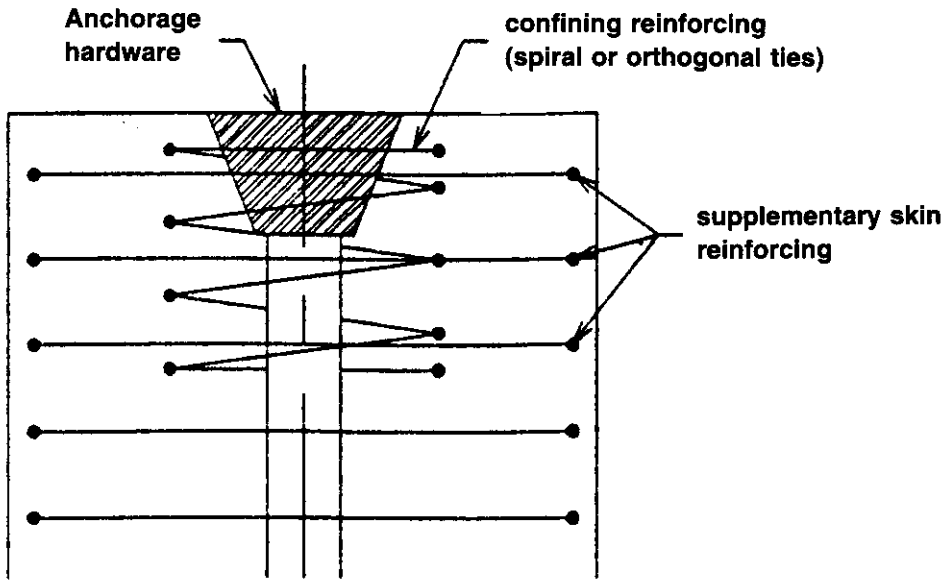

Figure 21. Definition of supplementary reinforcement.

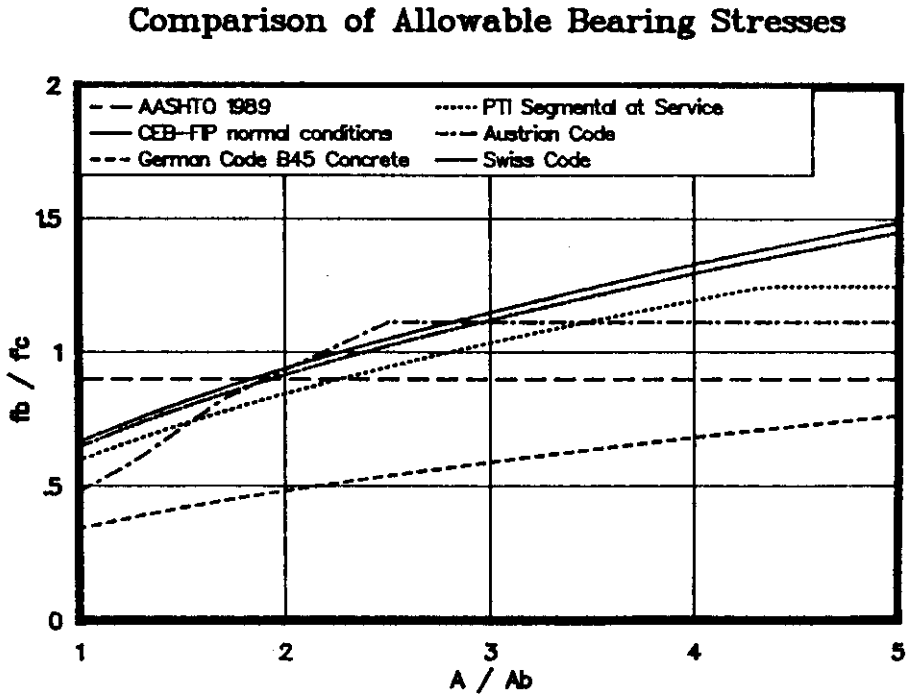

Figure 22. Comparison of code equations for bearing stresses.

dations for the Acceptance Application of Post-Tensioning Systems (3). The FIP outlines a test block (see Figure 25), test procedure, and criteria for evaluation. Side lengths, *m* and *n*, perpendicular to the tendon shall be taken as twice the permissible minimum distance from the center of the anchorage to the edge of concrete structure as recommended by the manufacturer (supplier). The height of the prism shall be twice the longer dimension, *m* or *n*, measured from the end of the device farthest from the load application. The test should be started when the concrete has reached approximately 85 percent of its characteristic strength (28-day cube strength), and strength gain should be limited so the characteristic strength is not exceeded during the course of the test. They recommend a cyclic or sustained loading procedure (see Figure 26) and ultimate limit state evaluation criteria.

Regardless of the test method chosen, the test must prove that

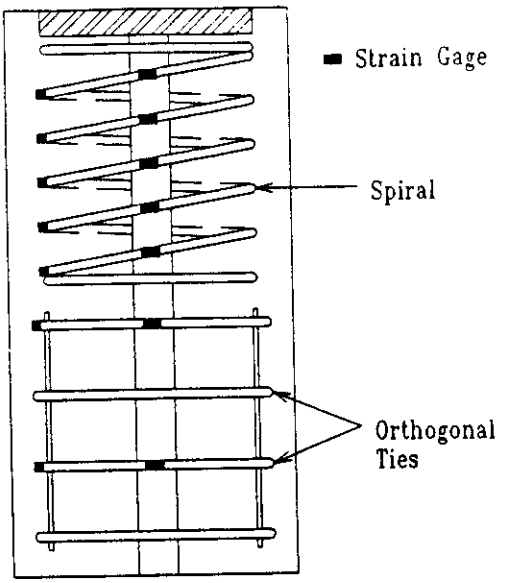

Figure 23. Typical strain gage layout.

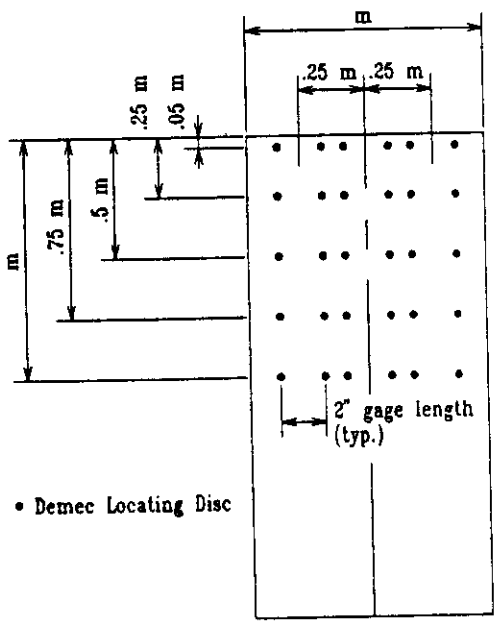

Figure 24. Typical Demec locating disc layout.

the anchorage zone is capable of transferring forces to the concrete without premature failure of the concrete or the bursting reinforcement. It must be designed in such a way that the maximum prestressing force is carried with an adequate factor of safety against failure. FIP also requires that the possible formation of small cracks in the anchorage zone not impair the permanent efficiency of the anchorage. The only other stipulation that FIP puts forth is that the minimum spacing of anchorages and minimum edge distance be determined in such a manner that the reinforcement can be easily placed, and that adequate compaction of the concrete is possible.

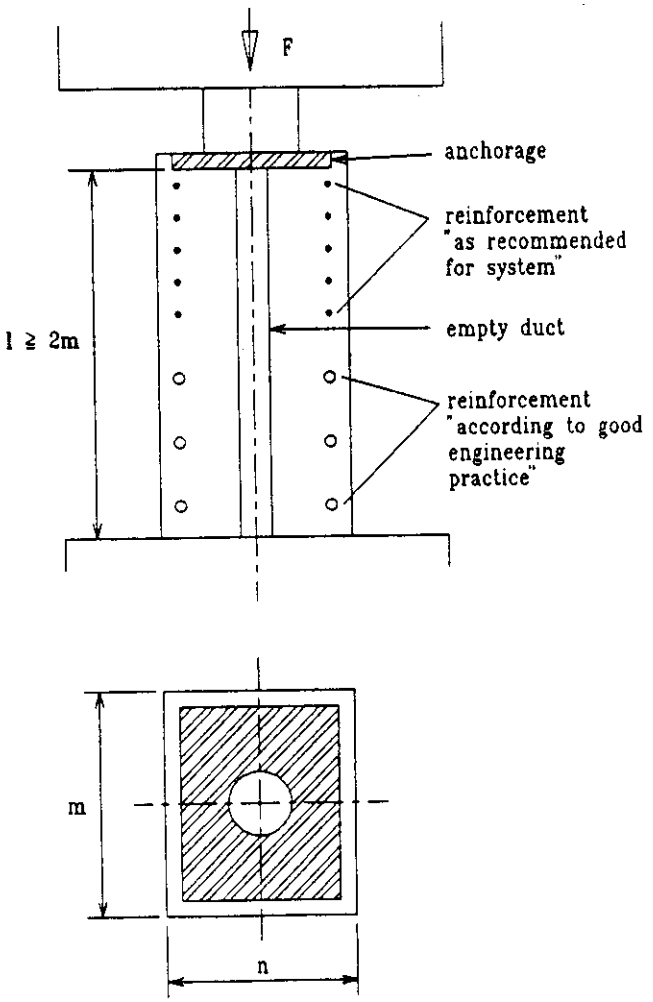

Figure 25. FIP test specimen.

The second test is described in the PTI specifications for segmental post-tensioned box girders (*17*), and is a significantly different acceptance test. The dimensions of the test block are somewhat different, the loading is monotonic, and serviceability (specific crack width), as well as ultimate criteria, are used for evaluation. PTI specifies a concrete prism with a cross-section dimension twice the minimum distance from the centerline of the tendon to the face of concrete in the actual structure in one direction, and equal to the minimum spacing of the anchorages plus 3 in. in the other direction (see Figure 27). The length of the test block is to be at least 1.5 times the largest cross-sectional dimension.

The specification further requires that the reinforcement in the anchor zone ahead of the anchorage, for a distance equal to the largest of the two cross-sectional dimensions of the specimen, shall simulate the actual reinforcement used in the structure. For the remaining length of the test block, the reinforcement may be increased as required to prevent failure in that portion. The strength of the concrete in the test block at the time of test must not exceed the minimum concrete strength at the time of post-tensioning.

The ultimate load criterion which must be satisfied is that the anchorage be capable of developing 95 percent of the guaranteed

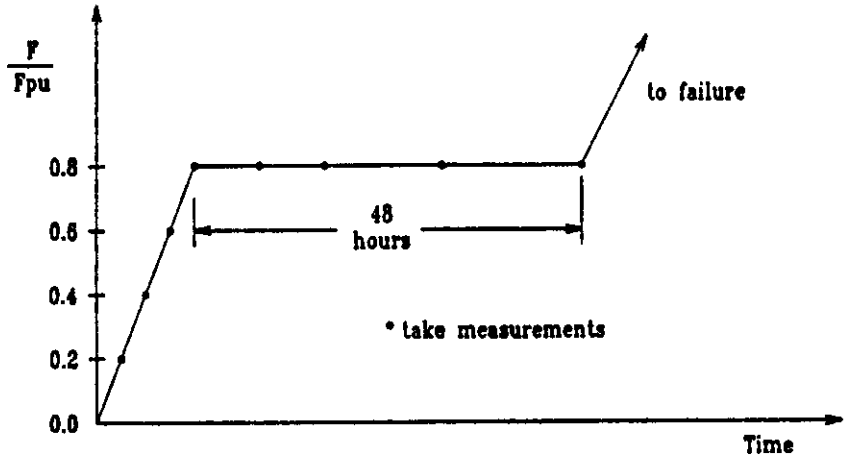

(a) Static Load Transfer Test.

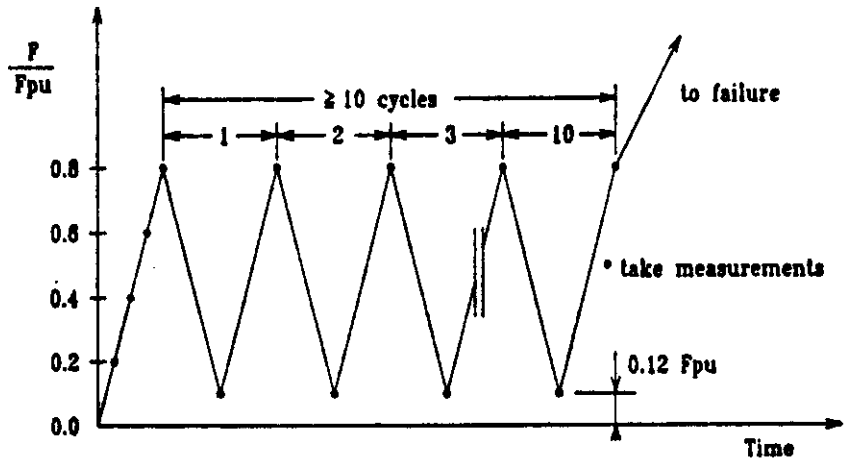

Figure 26. FIP loading procedure.

ultimate tensile strength of the maximum size tendon for which the anchor is rated, without measurable permanent distortion of the anchorage and without concrete failure. Measurable permanent distortion is defined as a distortion of 0.01 in. or more across the anchor face of the assembly measured from the original plane after the load has been released.

PTI also defines serviceability criteria. The test block must have no concrete cracks at a load of 40 percent F_{pu}, and concrete cracks at 70 percent F_{pu} must not exceed 0.005 in. After loading to 95 percent F_{pu} and releasing the load, concrete crack widths must not exceed 0.015 in.

These different procedures were evaluated by several series of tests. In test series MP (*M*ultiple *P*lane Anchors), six test specimens were built following the general outlines of the FIP procedures, but were loaded monotonically to failure. All specimens used a multiplane anchorage with a rated capacity of 12-0.6-in. diameter, 270-ksi strands. Manufacturer's literature required a minimum concrete strength of 3000 psi. MP-A had reinforcing details conforming to the manufacturers' European literature and allegedly proven in FIP tests. MP-B incorporated the spiral that is welded to the anchor when sold in the United States. MP-C and MP-E had details similar to MP-B but substantially higher concrete strengths. MP-D and MP-F were the same as MP-C and MP-E except three additional #4 supplementary ties were added to improve crack control. The rated capacity, F_{pu}, of the 12-0.6-in. strand anchor at a guaranteed ultimate tensile strength (GUTS) of 270 ksi is 700 kips.

Test results for the MP series are given in Table 1 along with a summary of the confining and supplementary reinforcing provided. The specimens incorporating the manufacturer's suggested configurations (MP-A and MP-B) failed to develop the rated ultimate capacity by substantial margins. At failure all of the anchorages had visibly depressed into the specimen's top bearing surface from $\frac{1}{4}$ to $\frac{1}{2}$ in. (see Figure 28). The concrete confined within the spiral confinement moved along with the anchor as it depressed into the concrete, as can be seen from Figure 29, taken when the spalled concrete was removed. The presence of supplementary skin reinforcement did little to improve the cracking load, which is substantially below the 0.80 F_{pu} temporary stressing level allowed by AASHTO. It appears futile to think of "uncracked" anchorage zones. The supplementary reinforcement did help in controlling crack widths, and a

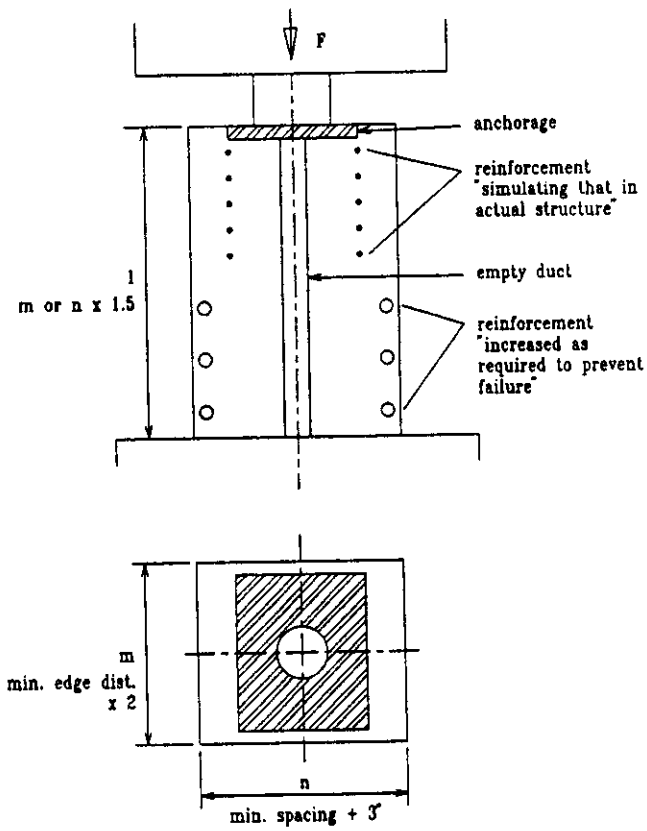

Figure 27. PTI test specimen.

Figure 28. Specimen MP-B anchorhead at failure.

comparison of MP-A and MP-B shows that the supplementary reinforcement can combine with the primary confining reinforcement to increase the ultimate capacity of the anchorage. Specimens MP-B, MP-C, and MP-E were identical in all details except for concrete compressive strength. Interestingly, first cracking was highest for the lowest concrete strength specimen. Ultimate loads increased at only about 90 percent of the increase in concrete strength.

Tests to Evaluate Acceptance Testing Procedures—Rectangular Plate Anchors

A similar investigation was carried out in the RP (*R*ectangular *P*late Anchor) series. Two specimens each with a 4-0.6-in. diame-

Table 1. Multiplane anchor test series

Specimen	f_c' psi[1]	Confining Reinforcing	Supplementary Reinforcing	Cracking Load	Ultimate Load
MP-A	3200	#4 spiral, 2-1/8 in. pitch, 5 turns	5 ea. #3 ties at 1-3/8 in.	0.46	0.81
MP-B	3200	#5 spiral, 2 in. pitch, 6 turns	None	0.46	0.63
MP-C	6400	Same as B	None	0.35	1.13
MP-D	6400	Same as B	3 ea. #4 ties at 4-1/2 in.	0.35	1.30
MP-E	4200	Same as B	None	0.30	0.80
MP-F	4200	Same as B	Same as D	0.30	1.05

[1] Manufacturer required: 3000

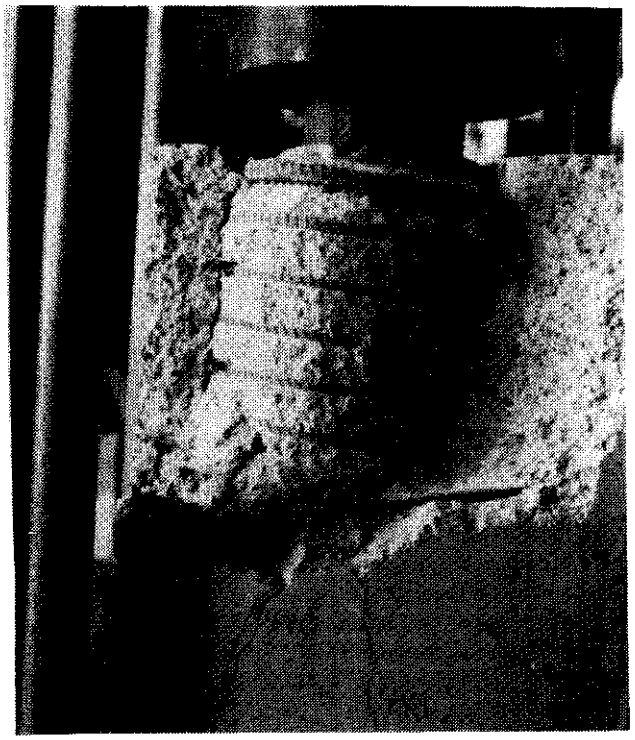

Figure 29. Specimen MP-B after failure.

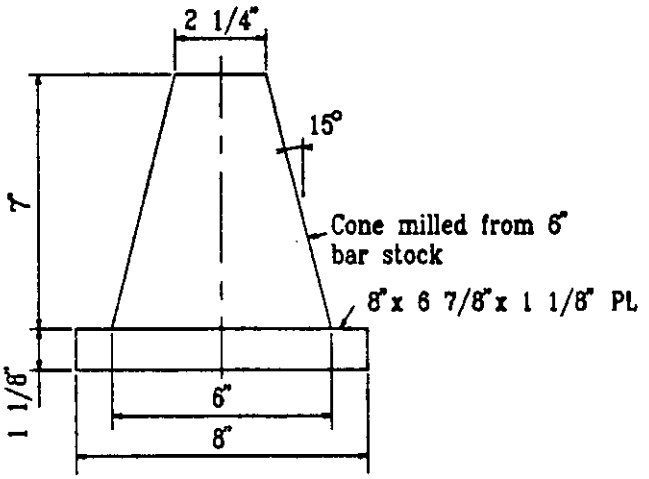

Figure 30. Anchorage device for specimens LH-D, E and F.

ter, 270-ksi strand rectangular plate anchor (F_{pu} = 232 k) were tested. Specimen RP-A had the manufacturers' recommended reinforcing details consisting of five #4 closed stirrups at $2\frac{3}{8}$-in. centers over the specimen cross section with three smaller additional #3 closed stirrups at $2\frac{3}{8}$-in. centers as additional confining reinforcement. Specimen RP-B had a $6\frac{1}{2}$-in. diameter #3 spiral with $1\frac{1}{4}$-in. pitch and nine turns. The spiral was sized to provide adequate confinement to the cone to develop F_{pu} using Richart's (*41*) approach. No other supplementary reinforcement was provided so that there was substantial concrete area without reinforcement. Test results are shown in Table 2. The rectangular specimen, RP-B, clearly indicated that a spiral arrangement of confining reinforcement is not always the optimum if not supplemented by reinforcing over most of the face of the specimen. The very large area of unreinforced concrete, from the perimeter of the spiral to the outside edges, developed very wide cracks, while the spiral developed less than 500 microstrain. The supplementary reinforcing in RP-A tied in the corners of the block and greatly enhanced the use of the confining reinforcing.

Test to Evaluate Acceptance Testing Procedures—Load History

The influence of *L*oad *H*istory was specifically investigated in the LH series. Loading histories included monotonic, cyclic, and 48-hour static load transfer tests. Two sets of specimens were used. In the first set (LH-A, LH-B, and LH-C) a "good" commercially available 4-0.6-in. strand rectangular flat plate anchor ($6\frac{7}{8}$-in. by 8-in.) was used with a confining spiral. In the second set a purposefully designed "bad" anchor was used to see if the test procedure would discriminate between "good" and "bad" anchors. This anchor was the same rectangular plate but had a heavy milled cone (see Figure 30) welded onto the

Table 2. Rectangular plate anchor test series

Specimen	f_c' psi	Confining Reinforcing	Supplementary Reinforceing	% F_{pu} (232 k)	
				Cracking Load	Ultimate Load
RP-A	3370	3 - #3 stirrups at 2-3/8 in.	5, #4 stirrups at 2-3/8 in.	0.64	0.97
RP-B	3370	#3 spiral, 1-1/4 in. pitch, 9 turns	None	0.43	0.82

Table 3. Load history test series

Specimen	Anchor	Load History	f_c'	Confining Reinforcement	Supplementary Reinforcement	Max. Crack Width at 0.80 F_{pu}	% F_{pu} (232 k)	
							Cracking Load	Ultimate Load
LH-A	Plate (good)	Monotonic	3900	#3 spiral, @ 2-in. pitch, 5 turns	None	0.005 in.	0.55	1.00
LH-B	Plate (good)	Cyclic	3900	Same as A	None	0.013 in. 0.125 in.[1]	0.50	0.96
LH-C	Plate (good)	Sustained	3900	Same as A	None	0.011 in. 0.017 in.[2]	0.55	1.12
LH-D	Cone (bad)	Monotonic	3900	Same as A	None	0.003 in.	0.45	1.15
LH-E	Cone (bad)	Cyclic	3900	Same as A	None	0.005 in. 0.125 in.[1]	0.45	1.15
LH-F	Cone (bad)	Sustained	3900	Same as A	None	0.009 in. 0.188 in.[2]	0.55	1.27

[1] 10 cycles

[2] 48 hr.

plate. The design of the anchor was based on the design of an anchor no longer being sold, which was known to have caused problems, such as excessive local zone cracking, in several structures. Test results are given in Table 3).

One of the basic conclusions, which can be drawn from this series, is that the ultimate failure load is not greatly affected by the loading history. Therefore, if ultimate load criteria are the only measure of performance, a simple monotonic testing procedure would be adequate. The level of distress, that is, the number and widths of cracks, is however greatly influenced by the method of test. The cyclic and sustained load tests showed the greatest amount of distress, while the monotonically loaded specimens showed the least. If serviceability criteria, such as crack widths, were to be considered in the evaluation of the test specimens, the sustained or slow cycle load transfer tests would better represent the conditions that would be present in a real structure.

From a testing standpoint, however, the sustained load transfer test is tedious and expensive. It is not always possible to tie up an expensive piece of testing equipment for the 48 hours required for this test. The slow cycle transfer test solves this problem very nicely. The levels of distress at the end of the sustained load and the cyclic loads were very similar. The cyclic test, therefore, is a viable replacement for the 48-hour sustained load test.

In terms of the "bad" anchor tests, it was interesting to note that the specimens with the stiff cones cracked earlier, but actually achieved higher ultimate loads than the identical anchors with flexible plastic transition cones. The difference in strength is attributable to the additional bearing area provided by the stiff cone. The cone increased the net bearing area by 19 percent and the average ultimate load increased by 15 percent, while the average cracking load decreased by 10 percent.

Tests to Evaluate Acceptance Testing Procedures— Multiple Bearing Plane Anchors

The final series for evaluation of test methods was the MB (*M*ultiple *B*earing Plane) series. Four identical specimens using a commercially available 7-0.5-in. 270-ksi strand anchor device were constructed with edge distance, spacing, and reinforcing details given by the manufacturer. The PTI test recommendations were used, resulting in a specimen 9 in. by 12 in. with a 24-in. height. The rated F_{pu} of the four specimens was 289 kips. MB-A and MB-B were unloaded, as specified by PTI, at 0.95 F_{pu}. They were subsequently loaded to failure. Specimens MB-C and MB-D were loaded continuously to failure. The specimens were tested at f_c' of 4100 psi.

Test results are given in Table 4. This was a very interesting series of specimens. There were basically two modes of failure illustrated in the four specimens and two distinct levels of ultimate load. MB-A and MB-C both failed very one-sided, with large diagonal cracks developing on only one side of the specimen. They failed at similar loads as well. MB-B and MB-D exhibited more symmetrical failures with the centerline cracks opening to greater widths and additional longitudinal, rather than diagonal, cracks developing.

What caused the difference in the failure mode is unknown. All four specimens were cast and tested identically. Small variations in positioning of the reinforcing steel or placement of the specimen in the loading machine could have been enough to make a difference. Once the slightly weaker path was found the one-sided failure occurred. The dimensioning of the specimen and the absence of auxiliary reinforcing tying in the corners seem to make the blocks very susceptible to the lopsided failure mode. The PTI specification forces a rectangular test specimen

Table 4. Multiple bearing plane anchor test series

Specimen	f'_c	Loading	Crack Width 0.70 F_{pu}	Confining Reinforcement	Supplementary Reinforcement	Residual Crack Width	% F_{pu} (289 k)	
							Cracking Load	Ultimate Load
MB-A	4100	Unloaded at 0.95 F_{pu}	0.005 in.	#4 spiral, 2 in. pitch, 5 turns	None	0.25 in.	0.55	0.96
MB-B	4100	Unloaded at 0.95 F_{pu}	0.005 in.	Same	None	0.10 in.	0.45	1.13
MB-C	4100	Continuous	0.010 in.	Same	None	0.25 in.[1]	0.45	1.00
MB-D	4100	Continuous	0.005 in.	Same	None	0.10 in[1]	0.45	1.08
						Average	0.48	1.04
						σ	0.04	0.07

[1] Actual (not residual)

for most anchors, which are square and have equal edge distances and spacings in each direction. Because most anchors are spirally reinforced, the specimen that results has more than 2 in. of extra unreinforced concrete in one direction. As seen in specimens MB-A and MB-C, when cracks open in this unreinforced area, they propagate and widen quickly. As a result, the specimen tends to fail at a lower load than one which fails more symmetrically.

This is the only series of this test program in which multiple specimens were constructed with identical details and tested with similar procedures. This presents the opportunity to examine the variability in first cracking and ultimate loads, which are inherent in the specimens because of the variable nature of reinforced concrete. Cracking loads were repeatable as were ultimate loads. Standard deviations were only 4 percent and 7 percent, respectively, which is very acceptable for any type of structural concrete test.

Tests for Parameter Studies

Many aspects of the local zone test specimens might have a significant effect on the behavior of the specimen and the outcome of the test. Effects of type of confining reinforcement and compressive strength of the concrete seemed to have been well explored in the literature. However, because of a shortage of documented test information, three areas were chosen for further study: edge distance, confining spiral parameters, and supplementary reinforcement.

Tests for Parameter Studies—Edge Distance

Test series ED (*E*dge *D*istance) used four specimens to isolate the effects of changing edge distance. Two used a 7-0.5-in. strand flat plate anchor and two used a 7-0.5-in. strand multiplane anchor device with an F_{pu} of 289 kips. All specimens were constructed using the manufacturer's recommended spiral parameters for B45 concrete, which corresponds to 6500 psi 28-day cylinder strength. The manufacturer's literature gave information for the reinforcing steel parameters for all of its anchors in a wide variety of concrete strengths. It then stated that for all cases the minimum edge distance is equal to one-half of the spiral diameter plus the cover according to local standards. According to AASHTO specifications for prestressed concrete the minimum cover over reinforcing steel is 1 in. for the bottom of slabs or over stirrups and ties. The maximum cover required is 2 in. for reinforcing on the top of slabs where de-icers may be used.

Using this information, for each anchor one specimen was built with transverse dimensions equal to the spiral diameter plus 2 in. and the other specimen had transverse dimensions equal to the spiral diameter plus 4 in. The specimens were dimensioned following the FIP recommendations and were loaded monotonically.

Test results are given in Table 5. As edge cover increases, the ratio A/A_b increases. It can be seen that with both types of anchors, this increase in edge cover increased the cracking load 20 percent. It increased the ultimate load 32 percent for multiplane anchors and 12 percent for flat plate anchors, and greatly reduced crack widths at both 70 percent and 95 percent F_{pu}. Thus, the edge cover used in an acceptance test is a critical decision and should be carefully chosen to be representative of applications.

Figure 31 shows load-deformation comparisons of the ED series specimens. These curves are typical of spirally confined local zone specimens and indicate reasonable ductility. They also indicate, as found by Wurm and Daschner (*38*), that the stiffness is only 7 percent to 15 percent of the expected stiffness based on the concrete elasticity modulus. Most of the deformation

Table 5. Edge distance test series

Specimen	Anchor	f'_c	A/A_b Ratio	Confining Reinforcement	Supplementary Reinforcement	Edge Cover	Crack Width (in.)		% F_{pu} (289 k)		
							70% F_{pu}	95% F_{pu}	Cracking Load	% F_{pu} Spiral Yield	Ultimate Load
ED-A	Multi-plane	5150	2.31	#4 spiral, 2 in. pitch, 4 turns	None	1 in.	0.005	0.188	0.50	1.08	1.10
ED-B	Multi-plane	5150	3.33	Same	None	2 in.	0.002	0.010	0.60	1.17	1.45
ED-C	Flat Plate	5150	1.54	Same	None	1 in.	0.004	0.015	0.50	1.18	1.24
ED-D	Flat Plate	5150	2.20	Same	None	2 in.	0.002	0.007	0.60	1.33	1.39

results from punching of the large, confined concrete plug into the prismatic specimen. Internal strain gages mounted on the spirals indicated that the spiral strains were well below yield at 0.95 F_{pu} (see Figure 32) for all specimens. As shown in Table 5, final failure occurred shortly after spiral yield for all specimens, except ED-B which had substantial extra load above spiral yield. This specimen had the largest A/A_b ratio and suggests that the extra confining concrete can enhance the effectiveness of the spiral confinement.

A very different level of strains is measured as longitudinal strain on the external face of the specimens. As shown in Figure 33, external strains dropped off fairly rapidly beyond a distance from the loaded face of 0.5 widths. Strains for specimen ED-A are not shown because they were so great they could not be measured with the Demec gage. They were approximately double the values shown for ED-B. With both types of anchors, the lower edge covers resulted in substantially greater external strains.

Figure 34 shows the development of splitting crack width with increasing load. The large diamonds shown on the figure are the PTI crack width criteria:

0.40 F_{pu}—no cracks

0.70 F_{pu}—crack widths less than 0.005 in.

0.95 F_{pu}—crack widths less than 0.015 in. after release of load

All specimens met all crack width criteria with the possible exception of ED-A at the 0.95 F_{pu} level. Load was not released, therefore, this could not be checked. However, in view of the very wide crack under load, it is unlikely that satisfactory recovery would occur.

Tests for Parameter Studies—Confining Spiral

In the SP (Confining *Sp*iral) series, the parameters of spiral pitch and diameter were altered while the spiral bar size and other specimen physical dimensions remained the same. In order to minimize the number of specimens, a previously tested specimen, ED-D, was chosen as the first specimen of this series. Three new specimens were constructed with the same anchor, a 7-0.5-in. strand flat plate anchor, concrete dimensions, base area reinforcing and approximate concrete strength. The only variable was the spiral. The first specimen, SP-A, had no spiral at all. The increased capacities of the three other specimens in the series above the failure load of SP-A could then be attributed entirely to the confinement provided by the spiral. Specimen SP-B had the same volumetric ratio of confining reinforcing steel to confined concrete as specimen ED-D, but the spiral diameter was increased from 8.25 in. to 10.25 in. Specimen SP-C had the same cross-sectional area of reinforcing steel in the spiral as ED-D, but an increased diameter. Test results are given in Table 6.

The provision of the spirals had a dramatic effect on the performance of the specimens. Specimens SP-C and SP-B, with 10.25-in. diameter spirals, had first cracking loads 45 percent higher than the unreinforced specimen, SP-A. Increased diameter of the spirals also helped somewhat since their cracking load was 9 percent higher than specimen ED-D. The spirals greatly controlled crack width. The provision of the spirals and especially the increase in spiral diameter also had a profound effect on the ultimate load.

Tests for Parameter Studies—Supplementary Reinforcing

Some of the manufacturers whose reinforcing details were studied during the course of this research recommended provision of supplementary (auxiliary) tie reinforcing in addition to the use of a spiral for primary confinement. Specimens in the MP series were tested with and without supplementary reinforcing. It was apparent that supplementary reinforcing significantly enhanced the ultimate strength of the specimen and also made the failure somewhat more ductile.

Series AR (*A*uxiliary *R*einforcing) was designed to observe the effects of varying the amount of supplementary reinforcing

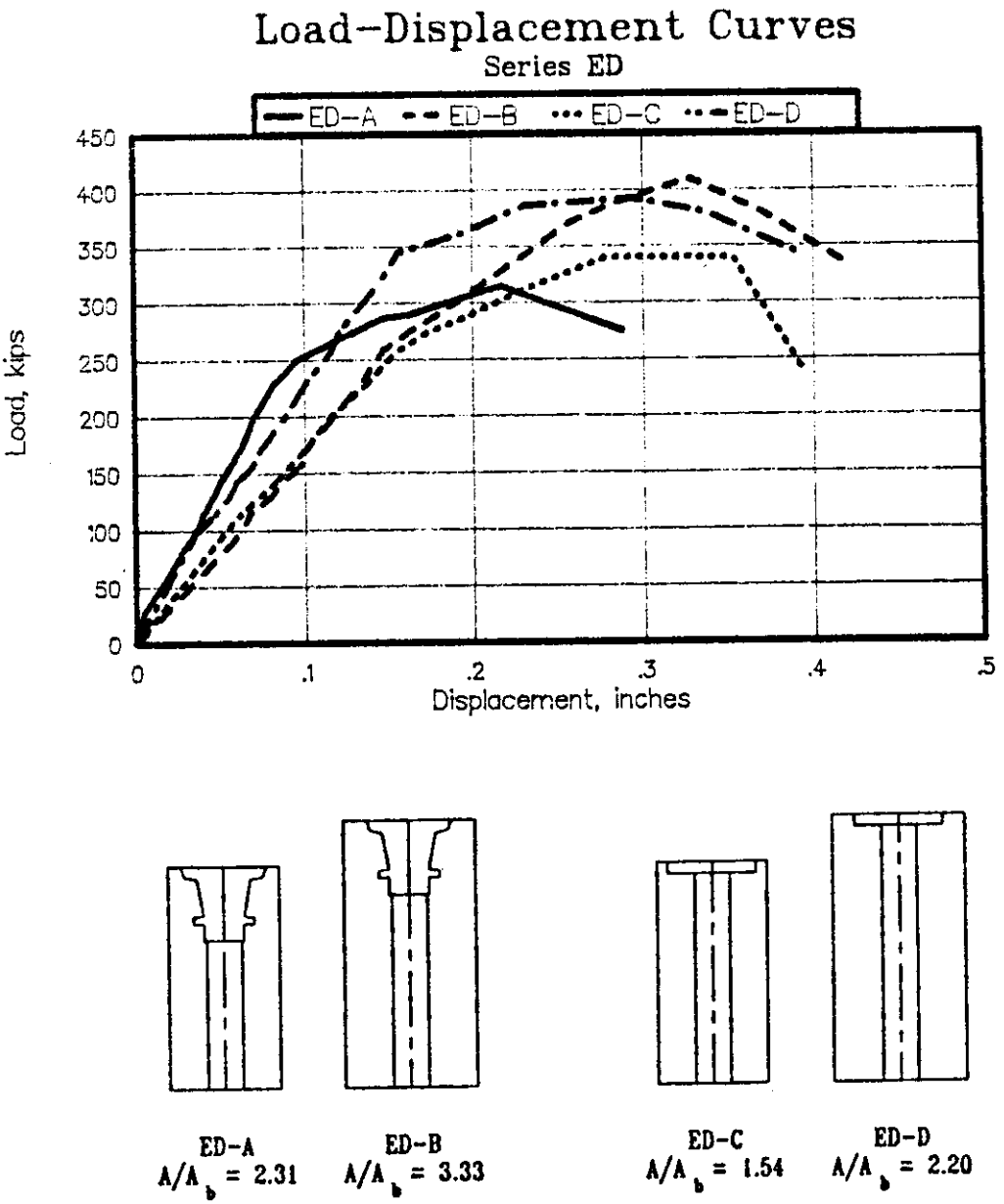

Figure 31. Load-deformation response for ED series.

in otherwise identical specimens. Specimen ED-A was chosen as the specimen whose basic parameters would be used for this series. The three new specimens were constructed with the same 7-0.5-in. strand multiplane anchor, same spiral and base area reinforcing, same concrete dimensions and approximate concrete strength as ED-A.

The AASHTO Bridge Specifications (*16*) gives a guideline for stirrups to be provided at the ends of prestressed beams in order to resist the splitting forces created by the transfer of the strand forces to the concrete. AASHTO recommends stirrups acting at a unit stress of 20 ksi to resist at least 4 percent of the total prestressing force. This guideline was used as the basis for the design of the specimens of this series. A 7-0.5-in. strand anchor has a capacity of 289 kips. Four percent of this is 11.6 kips. The cross-sectional area of steel required to carry 11.6 kips at a unit stress of 20 ksi is 0.578 in^2.

Specimen AR-A was designed with three #2 ties surrounding the spiral. This provided 0.30 $in.^2$ of cross-sectional area, which was one-half of the AASHTO recommendation. Specimen AR-B had three #3 ties. This provided 0.66 $in.^2$, which is just slightly greater than the AASHTO recommendation. The third specimen of the series, AR-C, had no local zone reinforcing. Test results are given in Table 7 and shown in Figure 35.

The first comparisons to be made are between the totally unreinforced local zone specimen, AR-C, and the specimen with only spiral confining reinforcing ED-A. The presence of spiral reinforcing dramatically improves the performance of the local zone specimen in terms of both ultimate load and crack width criteria, although the cracking load is less affected. Unlike the reinforced specimens that exhibit very wide cracking before failure, the unreinforced specimen failed quickly once the concrete began to crack. Table 7 shows that the first cracking load of

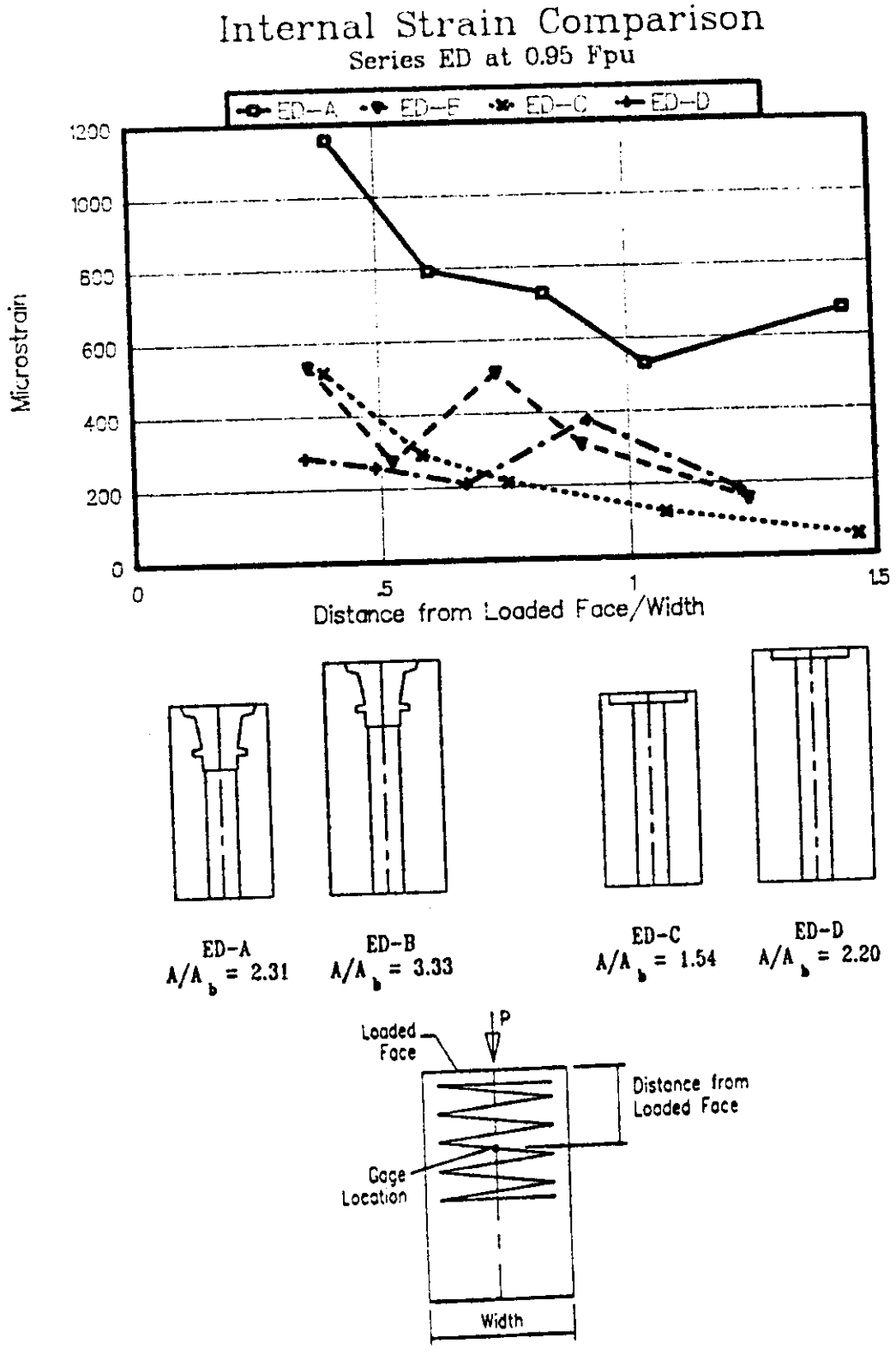

Figure 32. Spiral strains for ED series.

specimens with supplementary reinforcing was not significantly affected when compared with ED-A. However, the supplementary reinforcing did somewhat improve the ultimate load and substantially reduce the crack widths at high load levels.

Although supplementary reinforcement was clearly of substantial value in these acceptance test specimens, the final questions are whether the supplementary reinforcing needed for the anchor to pass the test requirement must be included in exactly the

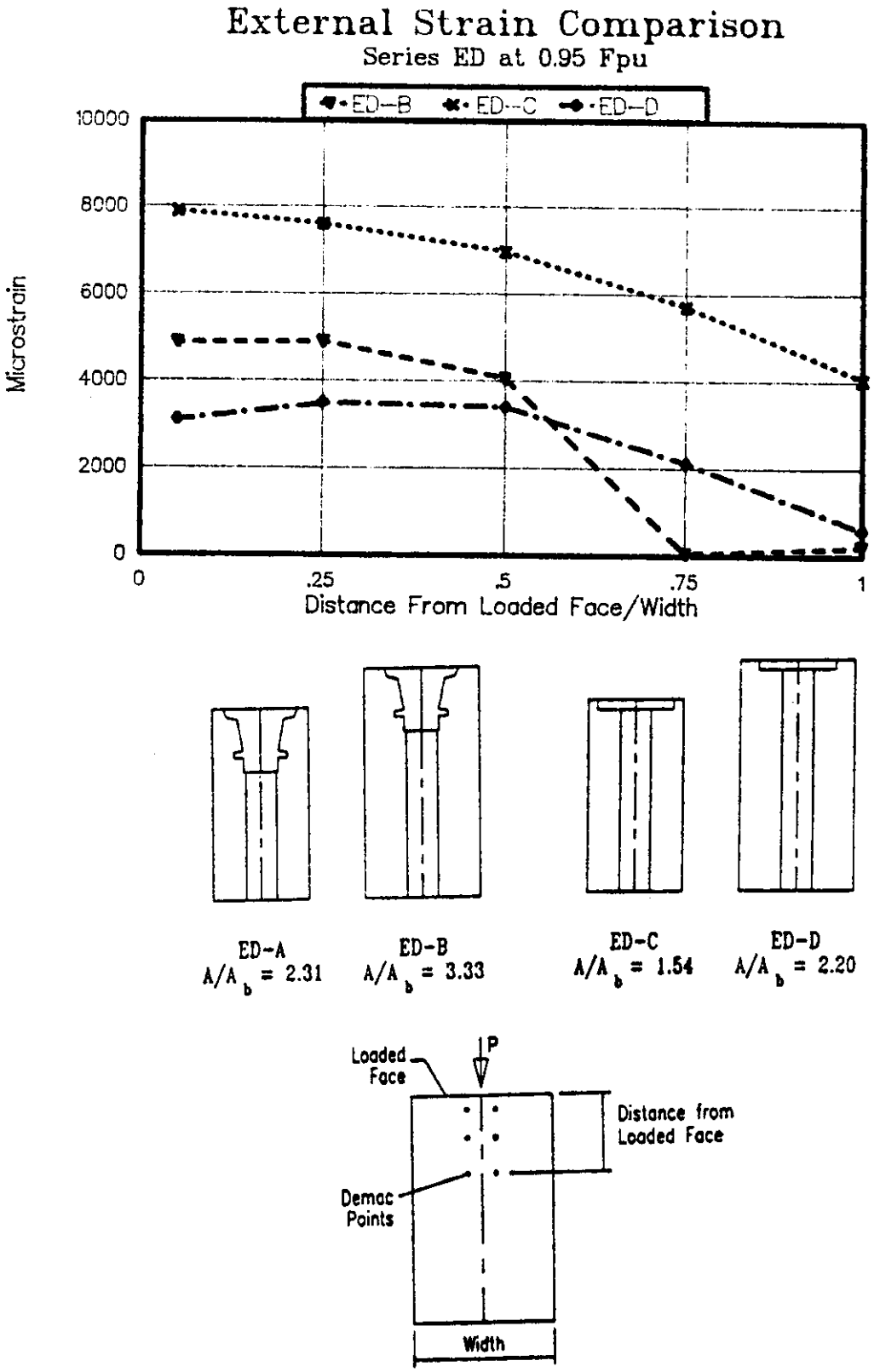

Figure 33. External strains for ED series.

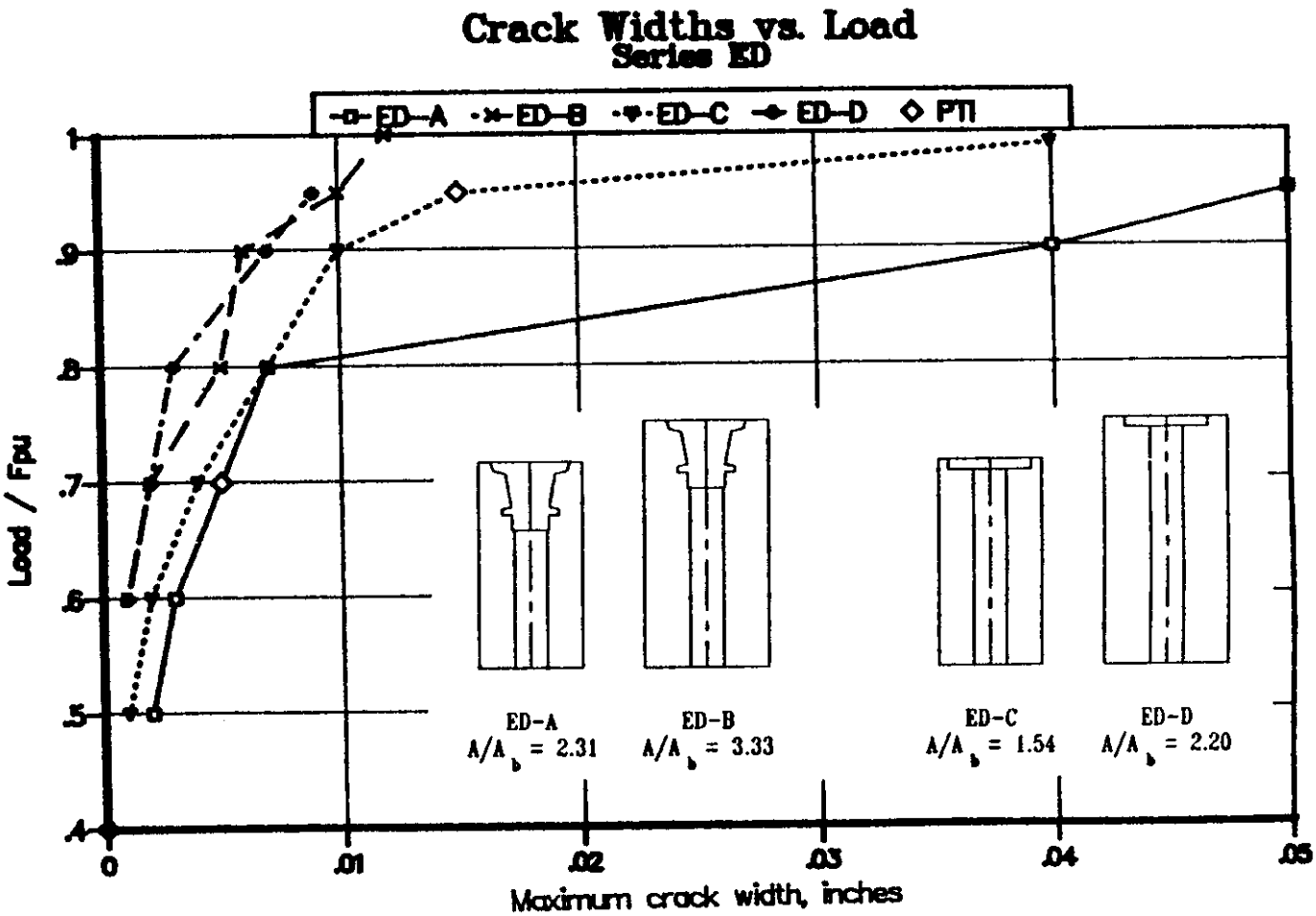

Figure 34. Crack width comparison for ED series.

Table 6. Series SP performance comparison

Specimen	f_c'	Spiral Parameters					Test Results			
							% F_{pu} (289 k)			
		Bar Size	Diameter (in.)	Pitch (in.)	No. Turns	Volumetric Ratio	1st Crack	Ultimate	Crack Width @ 70% F_{pu} (in.)	Crack Width @ 95% F_{pu} (in.)
ED-D	5150	#4	8.25	2	5-1/2	0.0540	0.60	1.39	0.002	0.007
SP-A	4800	N.A.	—	—	—	0.0	0.45	1.10	0.007	0.016
SP-B	4800	#4	10.25	1-1/2	7	0.0570	0.65	2.10	0.001	0.004
SP-C	4800	#4	10.25	2	5-1/2	0.0430	0.65	1.89	0.001	0.007

same form in a real structure or whether the function of this supplementary reinforcing could be performed by other reinforcing present in the local zone for other purposes, such as shear resistance or shrinkage control.

Local Zone–General Zone Interaction Tests

A fundamental assumption in the envisioned overall design strategy for post-tensioned anchorage zones is that the perform-

Table 7. Series AR performance comparison

Specimen	f'_c	Confining Reinforcing Details	Auxiliary Reinforcing Details				Test Results			
							% F_{pu} (289 k)		Crack Width at 70 % F_{pu} (in.)	Crack Width at 95% F_{pu} (in.)
			Bar Size	Side Length (in.)	Spacing (in.)	No. Ties	1st Crack	Ultimate		
AR-C*	5880	None	N.A.	—	—	—	0.40	0.80	0.007	N.A.
ED-A	5150	#4 spiral, 2 in. pitch, 4 turns	N.A.	—	—	—	0.50	1.10	0.005	0.188
AR-A	4825	Same	#2	7-7/8	2	3	0.50	1.13	0.002	0.030
AR-B	4825	Same	#3	7-7/8	2	3	0.45	1.25	0.003	0.007

* AR-C had no confining spiral

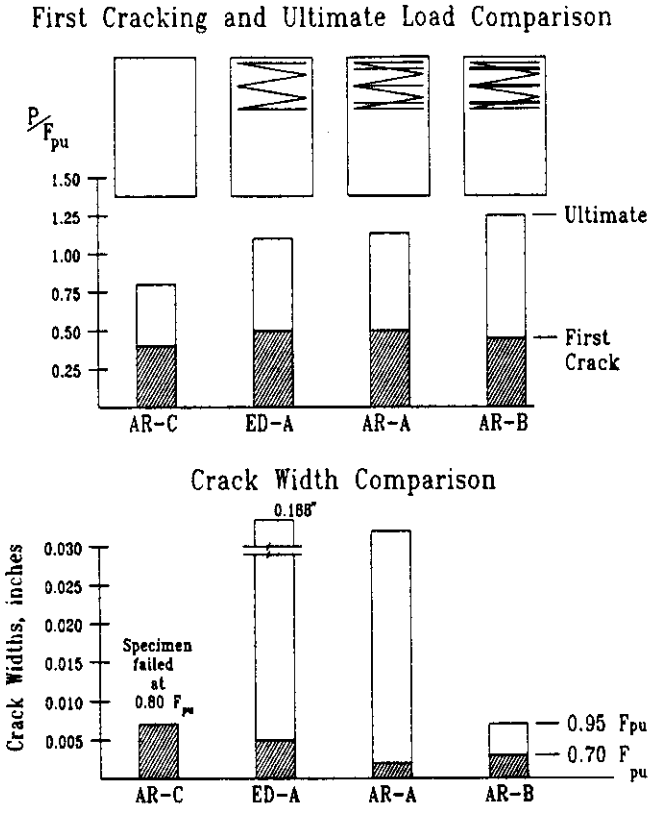

Figure 35. Series AR comparison.

ance of an anchorage device in a local zone test specimen will be a safe lower bound of its actual performance in the general zone of a more realistic bridge application. In this way, the acceptance criteria for the anchorage device could be satisfied by a limited analysis or acceptance test program without new verification having to be made for each new structural application.

The final series of specimens in the local zone program was the LG (*L*ocal Zone-*G*eneral Zone) Series. Three specimens were designed and constructed using the same local zone details as used in specimen ED-A with a 7-0.5-in. strand multiplane anchor with a #4 spiral and with 1-in. cover over the spiral. As shown in Table 7, it had first cracking load of 0.5 F_{pu} and very wide cracking (0.188 in.) at 95 percent F_{pu}, and it failed at 1.10 F_{pu}. In specimen LG-A, the anchor and the same confining spiral were placed in a concentric general zone situation; in LG-B they were placed in an eccentric situation and in LG-C they were placed in a multi-anchor specimen (specimen details are in Appendix C).

Specimen LG-A was designed using a simple strut-and-tie model. Bursting reinforcement was distributed over a zone extending from 0.19 h to 1.12 h. The bursting reinforcement bar sizes were proportioned to ensure that the general zone capacity would exceed the known capacity of the local zone test specimen, ED-A, which failed at 316 kips. Demec gages were placed on all the general zone specimens in the same pattern used in the local zone specimen.

Specimen LG-B was constructed with a single anchor placed eccentrically at the quarter point of the specimen. Spalling and bursting reinforcement were based on a successful specimen from the general zone test program, with the general zone reinforcing steel increased slightly to ensure that the general zone would not fail at a load lower than the known capacity of the local zone test specimen.

Specimen LG-C was a twin anchor concentrically loaded specimen with each anchor at the eighth point from the centerline. Details were based on previously tested general zone specimen.

In the comparison of results, data for specimen AR-B are also included. It had supplementary local zone reinforcement quite comparable to the portion of the general zone reinforcing which

Table 8. Series LG performance comparison

Specimen	f_c'	Specimen Configuration	Confining Reinforcing Details	Supplementary Reinforcing Area in Local Zone (si)	Test Results			
					% F_{pu}*		Crack Width at 70% F_{pu} (in.)	Crack Width at 95% F_{pu} (in.)
					1st Crack	Ultimate		
ED-A	5150	Local Zone Test Prism	#4 spiral, 2 in. pitch, 4 turns	None	0.50	1.09	0.005	0.188
AR-B	4825	Local Zone Test Prism	Same	0.66	0.45	1.25	0.003	0.007
LG-A	4800	Concentric General Zone	Same	0.44	0.50	1.38	0.003	0.010
LG-B	4800	Eccentric General Zone	Same	0.44	0.50	1.40	0.003	0.009
LG-C	4800	Multi-Anchor Specimen	Two of Same	0.62	0.70	1.20	0.001	0.003

* F_{pu} = 289 k except for LG-C, which has two anchors so F_{pu} = 578 k

passed through the local zone in the general zone test specimens. Test results are given in Table 8 and shown in Figures 36 and 37. They clearly indicate that the detail used in local zone specimen ED-A performed far better in the general zone specimens than in the local zone specimen. Furthermore, the general zone test specimens had equal or greater ultimate load capacities and comparable crack width control than the local zone specimen AR-B, even though there was less reinforcing in the local zone portions of the general zone specimens. This fulfills the requirement that the local zone test present a harsher environment for the anchorage than any it would experience in a real world application. It is interesting to note that specimen ED-A would have failed the PTI crack width criteria; yet, the detail performed quite adequately in the three general zone situations. This suggests that the local zone criteria may be unduly harsh for some anchors, if supplementary reinforcement is not used in the local zone test specimen as with AR-B.

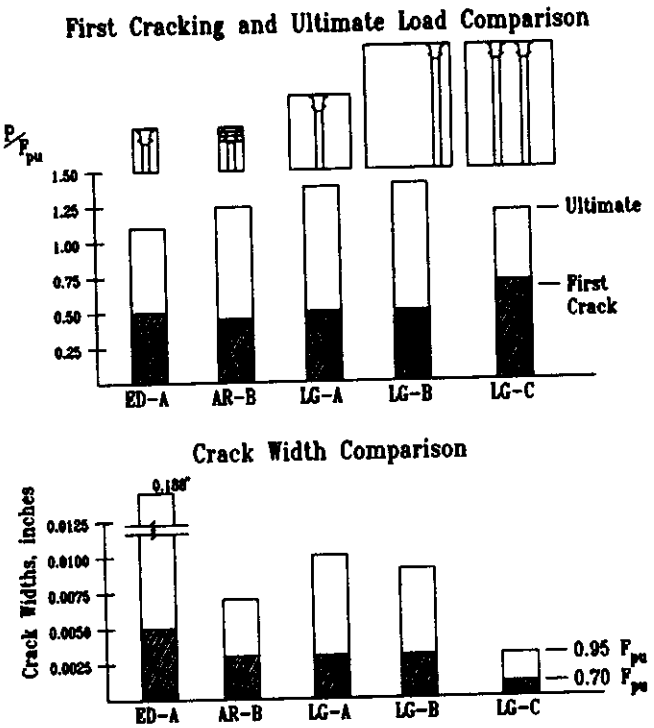

Figure 36. Series LG comparison.

Cracking Load Predictions

Historically, the first cracking load has been of interest to the designer, particularly when serviceability criteria are important. PTI (*17*), in its test specification, for example, requires that a specimen have no cracks prior to 40 percent F_{pu}. As pointed out previously, such criteria have little practical value in actual applications because in the United States design specifications permit temporary loading during stressing to 0.80 F_{pu}. A reliable method for prediction of first cracking might be used to screen

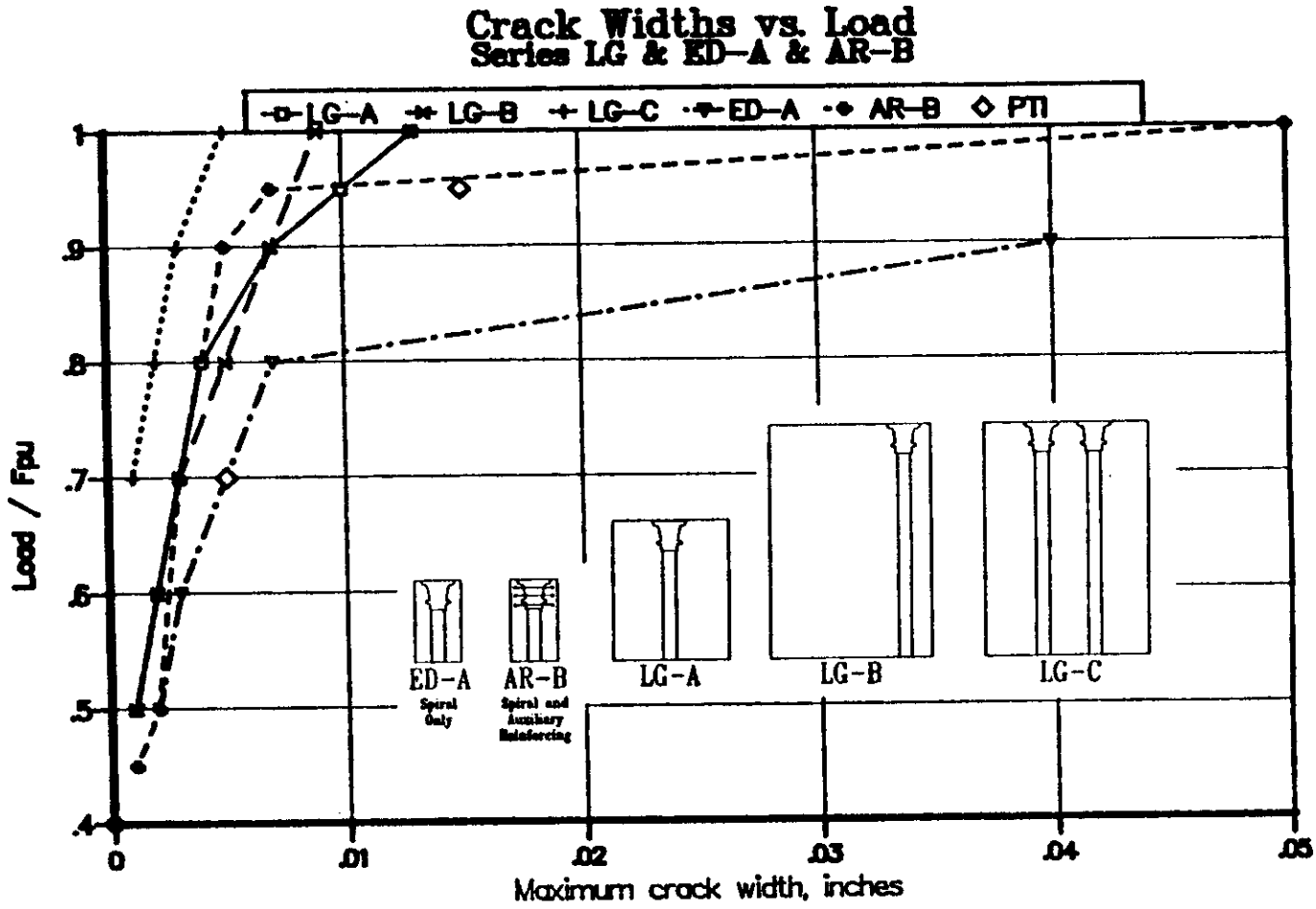

Figure 37. Crack width comparison for LG series.

anchorages proposed for use. Three widely reported crack prediction methods were evaluated as possible tools for estimating first cracking loads: (1) Guyon's (*6*) two-dimensional elasticity studies, (2) Yettram and Robbins (*42*) three-dimensional finite element (FEA) studies, and (3) Zielinski and Rowe's (*43*) experimental studies.

Roberts (*4*) pointed out that in past tests and theoretical analyses, the investigators used or assumed bearing plates over the entire specimen width and loaded by extremely stiff loading heads. The commercial anchorage devices in this study were loaded through smaller wedge plates as in actual usage. This changes the distribution of bearing stresses, as shown in Figure 38. Effective bearing areas were calculated, as shown in Figure 39, considering the effective bearing plate as circular and using the widely accepted principle of similar geometries to determine the effective area, A. These methods are not precise, but they do give a better estimation of the critical parameters, A_b, A, and a, for use in existing formulas.

Studies showed that critical tensile stress was best based on Ottosen's (*44*) three-dimensional failure criteria for concrete because of the high compressive stresses present under the plates. It was assumed that, at first cracking load, the maximum tensile stress predicted by the analysis procedure would equal the tensile capacity of the concrete, which was based on the previously measured split cylinder results adjusted by the Ottosen theory for the difference in stress state in a split cylinder specimen and in a local zone specimen (*4*).

The computed values are compared to the existing theories in Figure 40. Yettram and Robbins' three-dimensional FEA method is the most reasonable predictor for the local zone specimen with an average of 0.95 and a standard deviation of 0.19. Overall, it seems safe to say that an actual first cracking load will be well below Guyon's prediction and, quite probably, it will be above Zielinski and Rowe's conservative prediction.

Ultimate Load Predictions

There are two factors that have been proven in the past to have a great effect on the bearing capacity of concrete: (1) the A/A_b ratio and (2) the confinement by reinforcing steel.

Each of these variables was first studied independently by Roberts (*4*). However, she showed that the two work together in influencing the ultimate capacity of the local zone since the ultimate capacity is influenced by confinement provided by both the concrete and the reinforcing steel. Application of the bearing pressure formulas proposed by Hawkins (*13*), Billig (*45*), Komendant (*11*), and Williams (*37*) to the local zone specimens

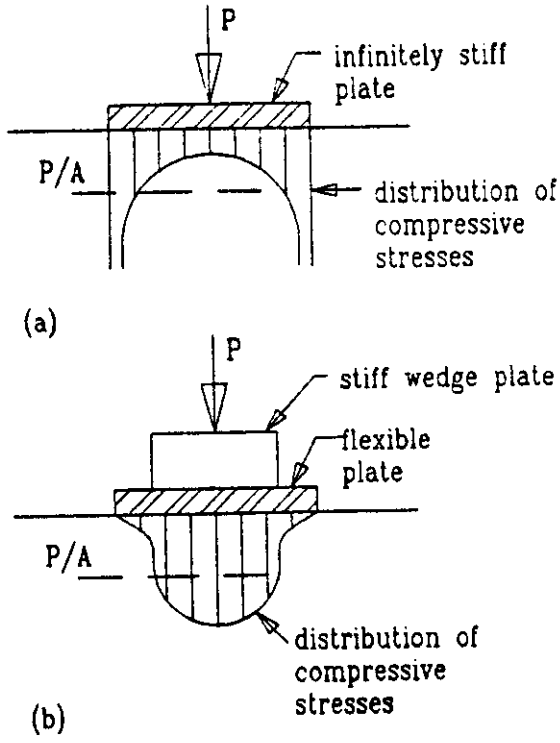

Figure 38. Stress distribution under bearing plates (from Roark, Ref. 62; Hawkins, Ref. 14).

of this investigation indicated conservative predictions, as shown in Figure 41. This is not surprising because all of the test specimens except two (SP-A and AR-C) had reinforcing in the local zone, while the bearing stress formulas were developed from tests on unreinforced concrete. However, it does indicate that present local zone approaches based on concrete bearing stress alone are not sufficient, because most commercial applications of anchorage devices for multiple strand tendons have confining reinforcement.

The effect of confinement on the ultimate capacity of the local zone specimens was also studied extensively by Roberts (*4*). The classic work by Richart et al. (*41*) was modified by Roberts to reflect the fact that the size and pitch of spirals typically used with anchorage devices do not produce the uniform confinement of the lateral oil pressure used by Richart. Roberts introduced a reduced confining pressure for square or rectangular ties that are often used in place of spirals (see Figure 42). She suggested that there will be arching of the confined concrete between spiral turns (see Figure 42c), so that a reduced area of compressive core should be considered. This area can be expressed as A_{core} $(1 - s/D)^2$. With this modification, the basic Richart equation would become

$$P_{ult} = A_{core}\,(f_c' + 4.1\,f_{lat})\,(1 - s/D)^2 \qquad (3)$$

This expression was used to compute the capacity of all the local zone tests. The ratio of test result to predicted capacity was a slightly unconservative 0.94 with a standard deviation of 0.21.

Further examination of the extensive work of Niyogi (*35,36*) and of Schlaich and Shäfer (*46*) indicated that the most effective

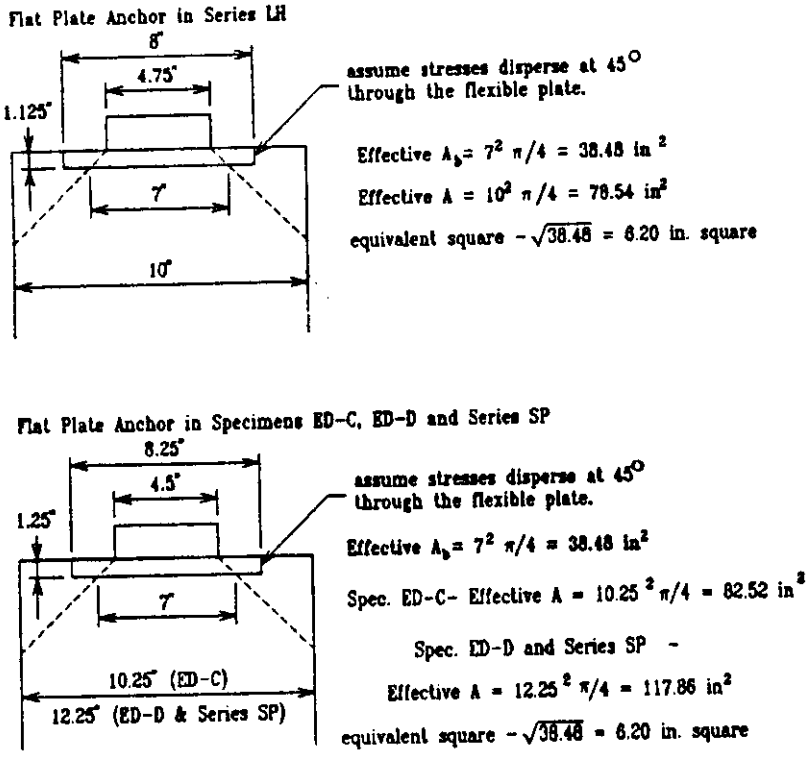

Figure 39. Calculation of effective bearing areas.

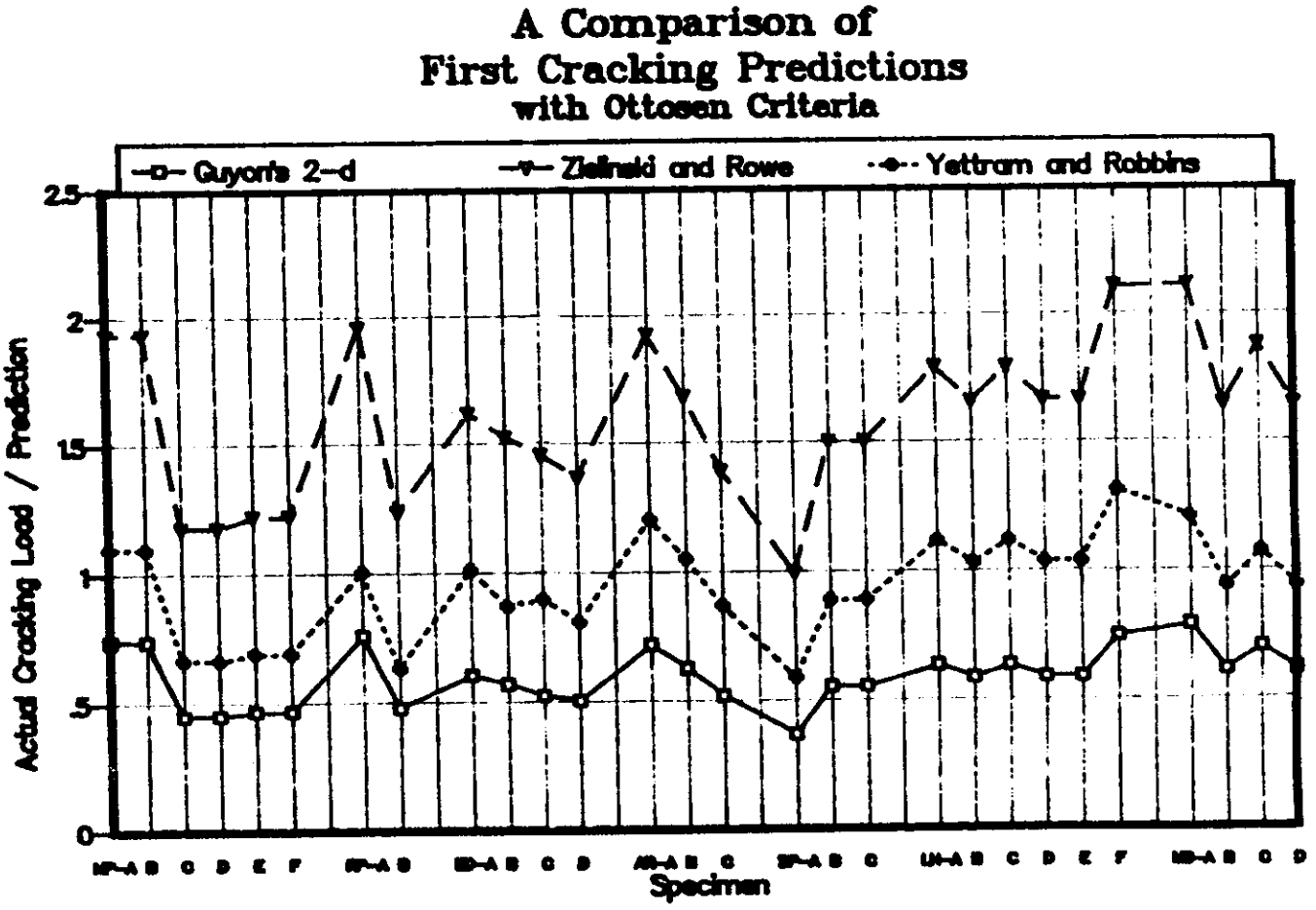

Figure 40. Comparison of first cracking predictions modified by Ottosen's criteria.

expression would be one which incorporated both the confinement of surrounding concrete (the A/A_b ratio effect) and the confinement provided by reinforcing (the f_{lat} effect). Wurm and Daschner (*39*) had found that there is an upper limit on the effectiveness of confining reinforcement (see Figure 43). Roberts suggested that since this limit seemed to be at $2A_s f_y/D_s = 1.2$, as shown in Figure 43, the corresponding limit on effective f_{lat} should be 1.20 ksi.

Roberts proposed that the ultimate load of local zones be computed as

$$F_{ult} = 0.80 f_c' \sqrt{A/A_b}\,(A_b) + 4.1 f_{lat} A_{core} (1 - s/D)^2 \qquad (4)$$

This predictive equation was compared to the local zone specimens of this study, the 27 reinforced specimens of Wurm and Daschner (*39*), and the 39 specimens of Niyogi (*35,36*) (see Table 9). The prediction was very good with an average of test/predicted of 1.03 and a coefficient of variation of 15 percent.

GENERAL ZONE ANALYSIS PROCEDURES

Introduction

Typical anchorage zones, as shown in Figure 44, are extremely complex. In this case there are four local zones, one around each anchorage device. The overall anchorage zone, or general zone as shown in Figure 15, would extend along the member for a distance equal to about the depth of the member, around 8 ft. Even the simplest possible geometry for an anchorage zone, a rectangular cross section loaded by a straight concentric tendon, is more complicated than it appears. The tendon duct causes a void in the structure, the reinforcement causes discontinuities in the material, and typical anchorage devices have a sophisticated geometry. Therefore, it is desirable to develop a general methodology for the analysis and the design of anchorage zones, rather than to attempt to define empirical expressions to solve the entire problem. Such expressions may be useful for certain cases within carefully defined limits.

At this stage of development of analysis procedures, the most likely candidates are: (1) linear elastic analysis (the older theory of elasticity approaches having been replaced by the much more versatile finite element analysis, FEA), (2) equilibrium based solutions (strut-and-tie models, STM), and (3) approximate equations.

Some studies using nonlinear finite element analysis have been published (*7*). As part of this project, such studies were also explored. At this stage of development they show some promise in explaining test phenomena, but they are not directly useful in design so they will not be treated explicitly in this report.

Frequently, anchorage zones are designed on the basis of a linear elastic analysis, such as Guyon's solution or finite element

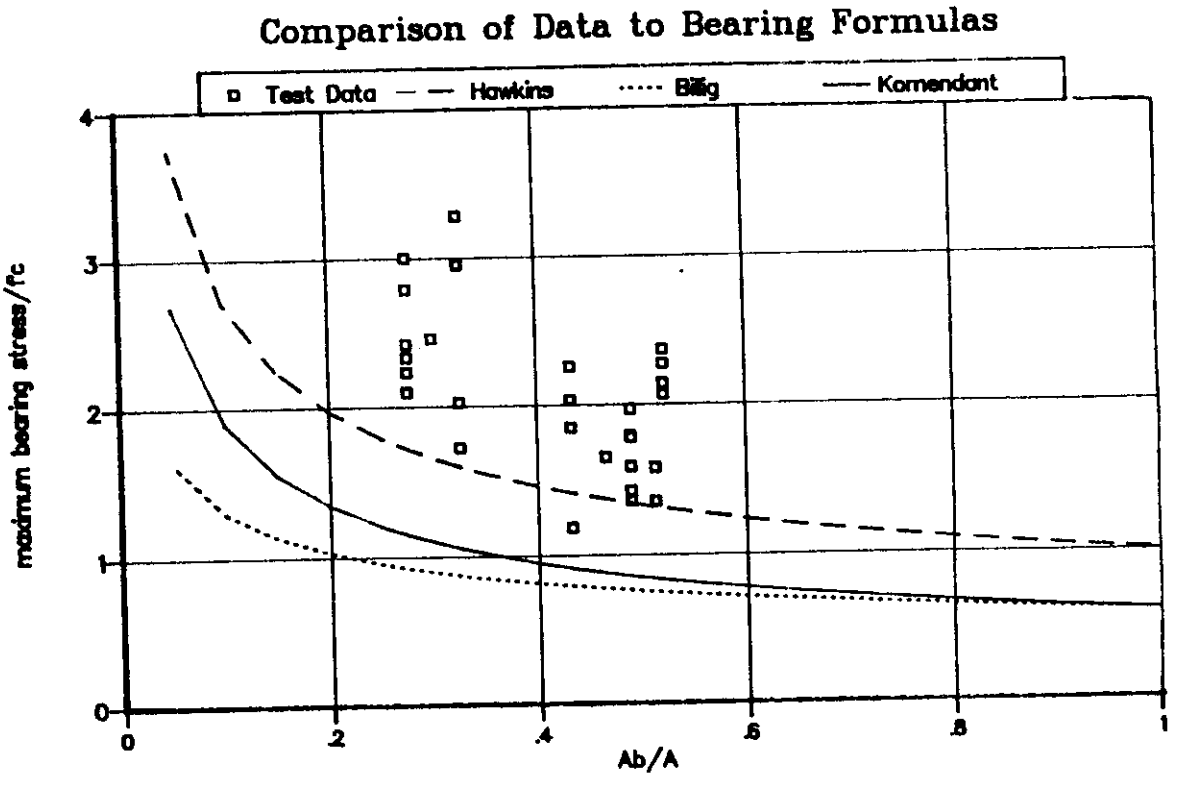

Figure 41. Comparison of bearing stress equations.

results, by integrating the transverse tensile stresses along the tendon path. However, the applicability of Guyon's solution is limited, and finite element analyses are involved and difficult to translate into reinforcement arrangements. Linear elastic finite element computer programs are widely available today, but their application to the analysis of cracked concrete is not entirely satisfactory. One of their main benefits is to indicate elastic force paths through plots of results as stress contours or stress vectors. In this way engineers can develop better understanding of the flow of forces for unfamiliar applications. For practical design applications, simple equilibrium-based solutions are very appealing to the design engineer (Figure 45). Such methods have become known as strut-and-tie models and have received wide attention lately.

Material Properties

As previously shown in Figure 15, the concrete is stressed over a large range, from extremely high compression in the vicinity of the anchorage to tension and possibly cracking in the general zone. Reinforcing steel is provided to confine the concrete surrounding the anchorage and to resist the tension forces that are released upon cracking of the concrete. Thus, the material properties of concrete and reinforcing steel must be carefully considered.

Although the concrete of the general anchorage zone is reinforced, the concrete in the general zone can generally be considered as unconfined except for the local zone. The absence of general zone confinement is not usually a major problem because, as shown in Figure 15, the compressive stresses decrease very rapidly with increased distance from the anchor. Because the concrete of the general zone is subjected to relatively low compressive stresses, in finite element analysis it is generally considered as a linear elastic material.

Unconfined concrete can resist compressive stresses in the vicinity of its uniaxial compressive strength f_c'. In beam bending, the limit value is $0.85\,f_c'$. For anchorage zones, where the state of stresses is more complex, the maximum value should be lower. The higher compressive strength of confined concrete was used in Eq. 4 in the discussion of the local zone.

Material models that assume perfect plasticity are commonly used in soil mechanics applications and efforts have been made to extend plastic analysis to structural concrete. The stress-strain curve of a perfectly plastic material exhibits an unlimited horizontal yield plateau, so that arbitrarily large strains without change of stress are possible after yielding (Figure 46). Collapse of a structure made of perfectly plastic material is characterized by the formation of a kinematic mechanism that allows unlimited deformations under constant stress. This collapse load or limit load can be bracketed by applying the lower bound theorem and the upper bound theorem, respectively. These limit theorems (*48*) say:

> Lower bound theorem: If an equilibrium distribution of stress can be found which balances the applied loads and is everywhere below yield or at yield, the structure will not collapse or will just be at the point of collapse.
>
> Upper bound theorem: The structure will collapse if there is any compatible pattern of plastic deformation for which the rate of work of the external loads exceeds the rate of internal dissipation.

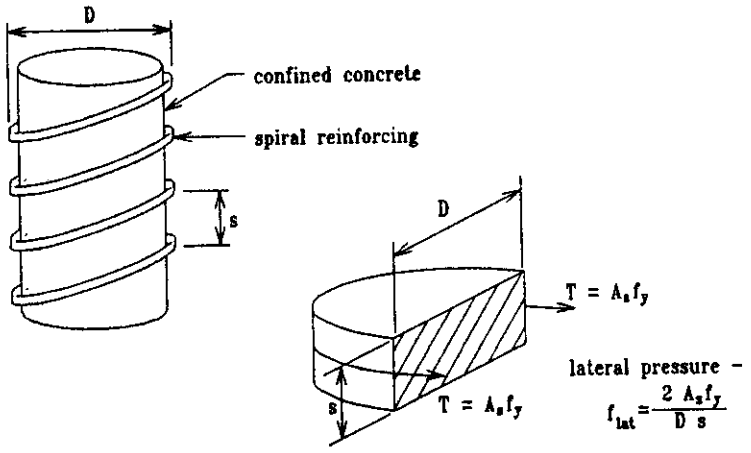

(a) Lateral pressure for spirals

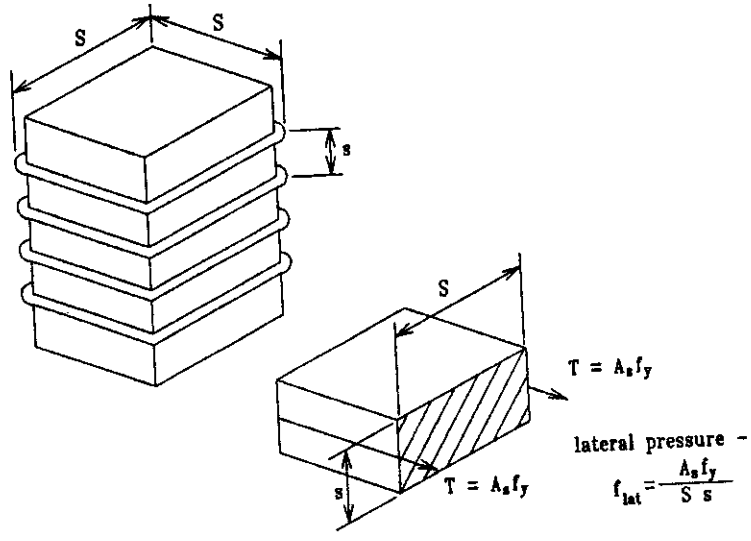

(b) Lateral pressure for ties

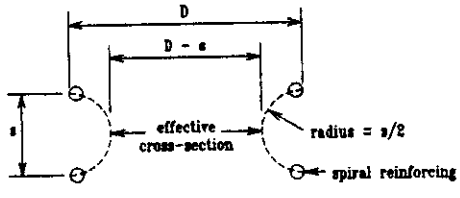

(c) Reduced spiral area

Figure 42. Calculation of lateral confining pressures.

The assumption of perfect plasticity is not particularly good for the description of the behavior of plain concrete because of the falling branch of its stress-strain curve and because of the limited ultimate strains. This is especially true for higher strength concrete. However, for reinforced concrete, and particularly for flexure of underreinforced members, plastic analysis works very well. The strip design method for slabs is an example for the application of the lower bound theorem, while yield line analysis is based on the upper bound theorem. But even if the concrete strength has a stronger influence on the limit load, good correla-

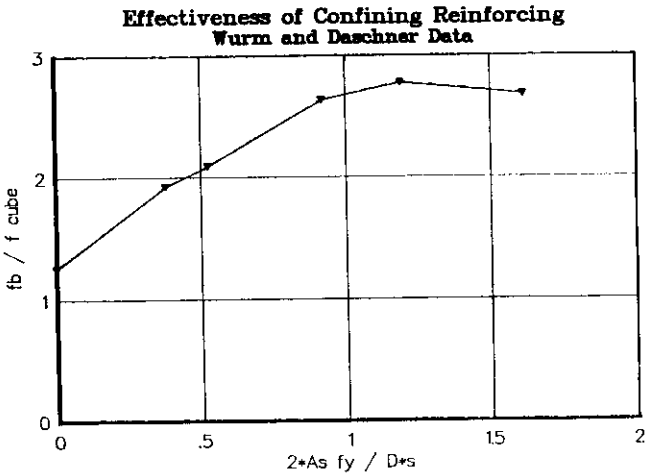

Figure 43. Effectiveness of confining reinforcing.

tion with test results can be achieved when a reduced "effective concrete strength" is taken into account. The reduction factor depends on a wide range of variables, such as concrete strength, tensile strains perpendicular to the compressive stresses, cracking, and geometry of the structure. Therefore, it has to be determined experimentally or estimated conservatively.

As shown in Figure 15, a large part of the anchorage zone is subjected to tensile stresses. Thus, the concrete of the general zone will be subjected to appreciable tensions. If the strains in the concrete reach the cracking strain, a crack opens and the tensile forces are transferred to the reinforcing steel. The tensile capacity of the concrete is generally neglected in design of an anchorage zone, because the concrete may crack during the lifetime of the structure due to other influences such as temperature or differential settlement. However, as will be demonstrated in the discussion of test results, this concrete tensile capacity can contribute substantially to anchorage zone strength.

In most cases, the reinforcement of the anchorage zone is provided by rolled deformed reinforcing bars of Grade 60. The confining reinforcement, if it is in the form of a spiral, is sometimes made of smooth bars of Grade 40 steel. Before cracking of the concrete, the strains in the reinforcing steel are very small, and most of the tensile forces are resisted by the tensile capacity of the stiffer concrete section. After cracking occurs, the forces that were carried by the concrete are transferred to the reinforcing steel. When the reinforcing steel reaches its yield strength, the force in the bars ceases to increase. Only when the strains in the reinforcement become significantly larger will the steel strain harden. In most cases, the extensive cracking and the large deformations required to reach strain hardening of the reinforcement are not attained before another mode of failure takes place, or before ductility of the anchorage zone is exhausted. For the study of anchorage zones, the reinforcing steel therefore, can be considered as a bilinear material exhibiting a perfectly elastic behavior up to its yield point, and a perfectly plastic behavior beyond that point.

Three-Dimensional Effects

All structures are three-dimensional. However, in many instances they can be represented using a simpler geometric model, such as a linear member for a beam. In anchorage zones, the concentrated force introduced by an anchorage device must be distributed to the entire cross section of the member, requiring a three-dimensional spreading of the forces. As a simplification, it is often sufficient to consider the spreading of the forces in two principal planes perpendicular to each other. In the simplest case of the distribution of a tendon force over a rectangular cross section, the spreading of the post-tensioning force can be considered separately in the main plane of the structure (largest dimension) and over the thickness.

In many cases in which post-tensioning is used, the cross section of the member is not a simple rectangle. Rather, it can be described as an assemblage of elements, each of which can be approximated as a thin rectangular cross section. Even though the overall problem is three-dimensional, the state of stresses in each component of the structure is essentially planar, with the exception of the local zone and the interfaces between the various components.

As an example, Figure 47 shows the case of the box-girder bridge The top and bottom flanges, as well as the webs, can be considered as rectangular components of the cross section and the spreading of the tendon force can independently be investigated on each of the components of the cross section. This method of breaking down the section into planar elements was proposed by Schlaich et al. (*2*) and was successfully used in this project.

Finite Element Analysis

The finite element method has become increasingly popular for calculating the detailed state of stresses in structures of arbitrary shape. Modern computer programs allow the user to model arbitrary structures and to define sophisticated material laws for the model. Figure 48 shows an example of a finite element mesh, showing the subdivision of the anchorage zone into quadrilateral elements. Burdet (*48*) has reported in detail on proper modeling of anchorage zones including information on convergence, accuracy, and variability as influenced by mesh size, number of nodes, and assumptions as to bonding between the anchorage device and the concrete.

Application of the finite element method is often limited by the lack of appropriate models for the behavior of the materials. This is especially true of the modeling of cracks in concrete. Cracks are usually not modeled as discrete discontinuities that extend as the load increases. Instead, the crack is considered as smeared over the considered elements, accordingly decreasing their stiffness (*49*). While this hypothesis may be acceptable for large structures with a uniform distribution of reinforcement, it is much less accurate for small regions of reinforced concrete structures where the stresses in the reinforcing steel vary sharply at the cracks, as is the case for anchorage zones. Finite element modeling of structural concrete is very much a field of research and rapid development at the present time (*50*). For this research, the Finite Element Program ABAQUS (*51*) was used to perform the stress analysis. The generation of the finite element models was performed using PATRAN (*52*), a general purpose preprocessor for finite element analysis.

The vast majority of analyses performed during this phase of the project were linear elastic. This choice was made to simplify the individual analyses, allowing a wider range of geometries

Table 9. Comparison of prediction equations with test data

Roberts (4) Specimen	Test/Eq.	Wurm & Daschner (38) Specimen	Test/Eq.	Niyogi (34, 35) Specimen	Test/Eq.
MP-A	0.70	13	1.14	B11	0.98
MP-B	0.69	19	1.03	B12	1.00
MP-C	0.82	25	1.14	B13	0.95
MP-D	0.94	14	0.92	B14	0.97
MP-E	0.75	20	0.94	B15	0.98
MP-F	0.96	26	0.96	B16	1.00
RP-A	0.64	15	1.14	B17	1.13
RP-B	0.75	21	1.19	B18	1.11
ED-A	0.93	27	1.31	B21	0.72
ED-B	1.10	16	1.16	B22	0.76
				B23	0.80
ED-C	0.93	22	1.13	B24	0.86
ED-D	0.94	28	1.12	B25	0.94
AR-A	0.99	18	1.08	B26	1.02
AR-B	1.10	24	1.08	B27	1.18
AR-C	0.97	30	1.05	B28	1.09
SP-A	1.23	36	1.17	B31	0.64
SP-B	1.10	37	1.12	B32	0.76
SP-C	1.05	38	1.20	B33	0.77
LH-A	0.74	35	1.14	B34	0.85
LH-B	0.71	39	1.09	B35	0.91
LH-C	0.83	40	1.13	B36	1.07
LH-D	0.90	33	1.33	B41	0.82
LH-E	0.90	34	1.31	B42	1.12
LH-F	0.99	41	1.30	B43	1.01
MB-A	0.97	31	0.95	B44	1.22
MB-B	1.12	32	0.92	B45	1.29
MB-C	1.00	42	0.93	B46	1.44
MB-D	1.07			B47	1.48
				B48	1.78
				S11	1.10
				S12	0.99
				S13	0.84
				S21	0.93
				S22	1.01
				S23	0.90
				S24	1.00
				S25	0.91
				S26	1.09
Average	0.92	Average	1.11	Average	1.01
Max.	1.23	Max.	1.33	Max.	1.78
Min.	0.64	Min.	0.92	Min.	0.64
Std. Dev.	0.15	Std. Dev.	0.12	Std. Dev.	0.22
Coef. Var.	0.163	Coef. Var.	0.107	Coef. Var.	0.215

and load configurations to be investigated analytically. An exploratory study of nonlinear finite element analysis was used to more closely investigate some specific configurations.

Simplifying hypotheses are necessary for the analysis of the very complex behavior of anchorage zones. The simplest model is to assume the material to be linear elastic. Because the stresses in the concrete and the reinforcing steel are generally small up to the cracking of the concrete, a linear model is quite accurate to describe the behavior of the general zone of a specimen up to cracking. Reasonable estimates of the cracking load of the general zone, therefore, can be obtained from a linear elastic stress analysis. The accuracy of the cracking load predictions could be influenced by the very large compressive stresses in the local zone. However, the presence of confining reinforcement is presumed to minimize this effect.

As will be shown, the results of a linear elastic finite element analysis can also be successfully used to determine the required amount of tensile reinforcement and to estimate the maximum compressive force that can be applied on an anchorage zone. Regardless of the method used to obtain the required amount of reinforcement, it is often desirable for effective crack control to pattern the tensile reinforcement somewhat according to the elastic stress distribution.

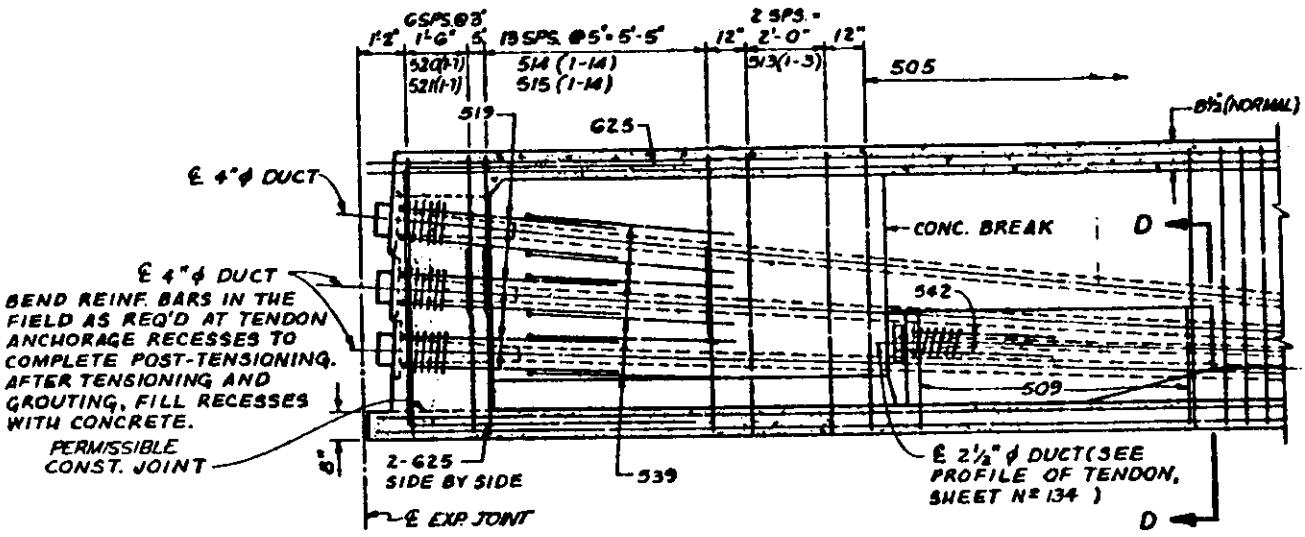

Figure 44. Typical anchorage zone with four tendons.

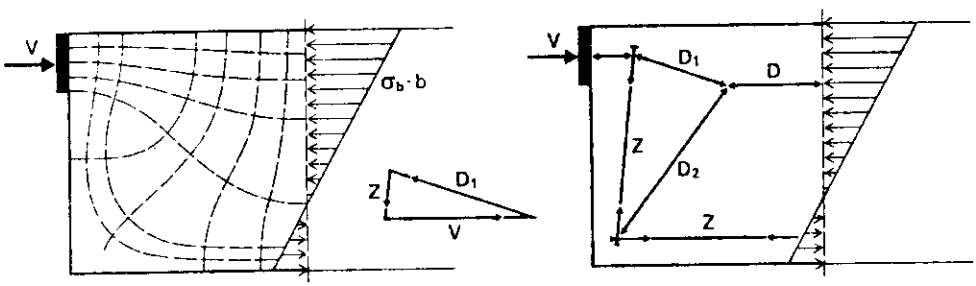

Figure 45. Flow of forces in anchorage zone.

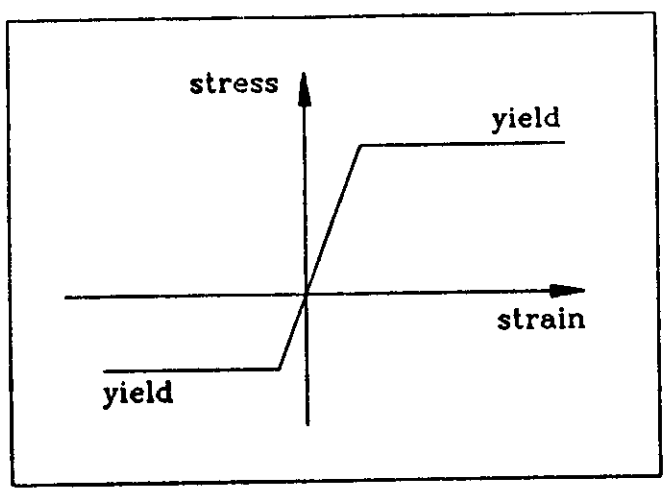

Figure 46. Elastic-plastic stress-strain curve.

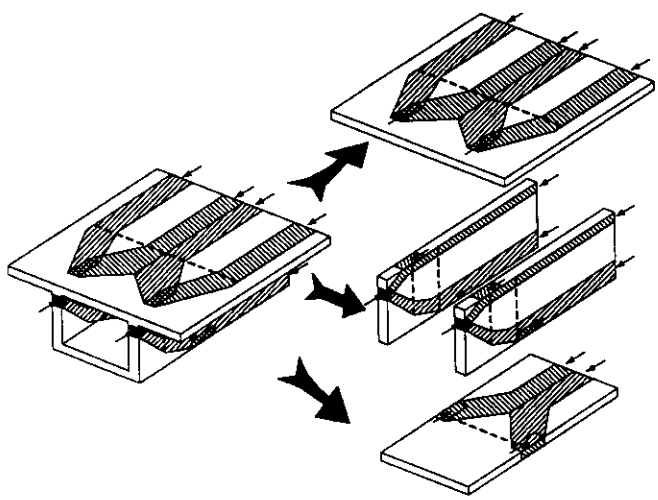

Figure 47. Principle of decomposition of a complex cross section into principal planes.

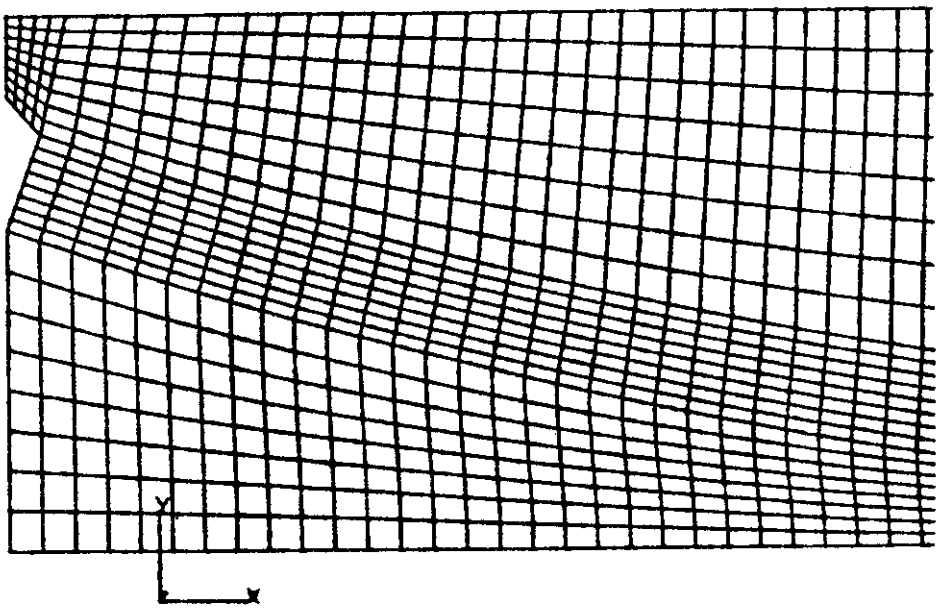

Figure 48. Example of two-dimensional finite element mesh of an anchorage zone.

Once a finite element analysis has been performed, it is best to represent the stress distribution in graphical form. Several representations exist. Because stress is a second-rank tensor, it seems best to combine several representations to present the results for evaluation.

A contour plot, as shown in Figure 49, is a plot of lines of equal stresses. However, because a stress function has several components, contour plots of one component give an incomplete picture of the state of stresses. In plane stress analysis, for example, a total of three contour plots is necessary to represent the three components of stresses in the plane. Despite their limitations, contour plots are helpful, especially for simple configurations. One single plot of the stresses normal to the tendon path can yield sufficient information to design the bursting reinforcement for the general anchorage zone. Both ABAQUS and PATRAN offer facilities to generate contour plots of the stresses.

An X-Y plot, such as the one shown in Figure 50, can be used to show the stresses perpendicular to the axis of the tendon. A comparison is made between the results of the three-dimensional analysis and the plane stress analysis. They are seen to be practically identical.

Isostatic lines, as shown in Figure 51, are lines that are at all points tangent to the direction of the principal stresses. They are similar to the equipotential lines of a flow net plot for underground fluid flow. Isostatic lines correspond to the intuitive idea of "spreading of forces" through a body. As a matter of fact, it is relatively easy to "guess" and draw isostatic lines for a simple configuration.

The tensorial nature of the stress function, in contrast to the scalar potential in fluid flow, renders an automated computation of isostatic lines complicated. However, a plot representing a field of principal stress vectors, as shown in Figure 51, gives a visual idea that is very close to isostatic lines. The generation of principal stress vector plots can easily be automatized. If isostatic lines are desired, they can be drawn tangent to the corresponding vectors. If the vectors are scaled so that their lengths represent the magnitude of the stresses, plots of principal stress vectors also give indications of the relative magnitude of the stresses.

A program to process the results of the finite element analysis and to display the principal stress vectors and X-Y plots was developed by Burdet (*48*) on a microcomputer. This program allows a quick and easy interpretation of the results of a finite element analysis and can export the results in several common file formats for further treatment. Because the program is based on a microcomputer and is user friendly, it was extensively used in the design of specimens to evaluate the various design options.

The results of a linear elastic analysis of the anchorage zone can be used for the design of the reinforcement in the general zone. Placing an amount of reinforcement, corresponding to the calculated elastic tensile forces, in the locations where the stresses in the concrete exceed the tensile strength, allows an immediate load transfer when cracking occurs. The method of systematically placing reinforcement to resist any tensile stress in the model has often been used and is generally conservative. Furthermore, because the reinforcement is located exactly where it will be needed, it is expected that such a procedure will limit the extent of cracking. The knowledge of the elastic state of stresses in an anchorage zone is, therefore, a good starting point for design of reinforcement.

The compressive capacity of the anchorage zone can be estimated by computing the level of compressive stresses in the concrete under the factored tendon force. Because the confining reinforcement of the local zone generally extends for a length approximately equal to the lateral dimension of the anchorage device, the present study limits the stresses in the concrete at that location ahead of the anchorage device to $0.70 f_c'$.

Strut-and-Tie Models

Today's strut-and-tie model procedures have evolved from the truss model for shear design. Although the truss model was

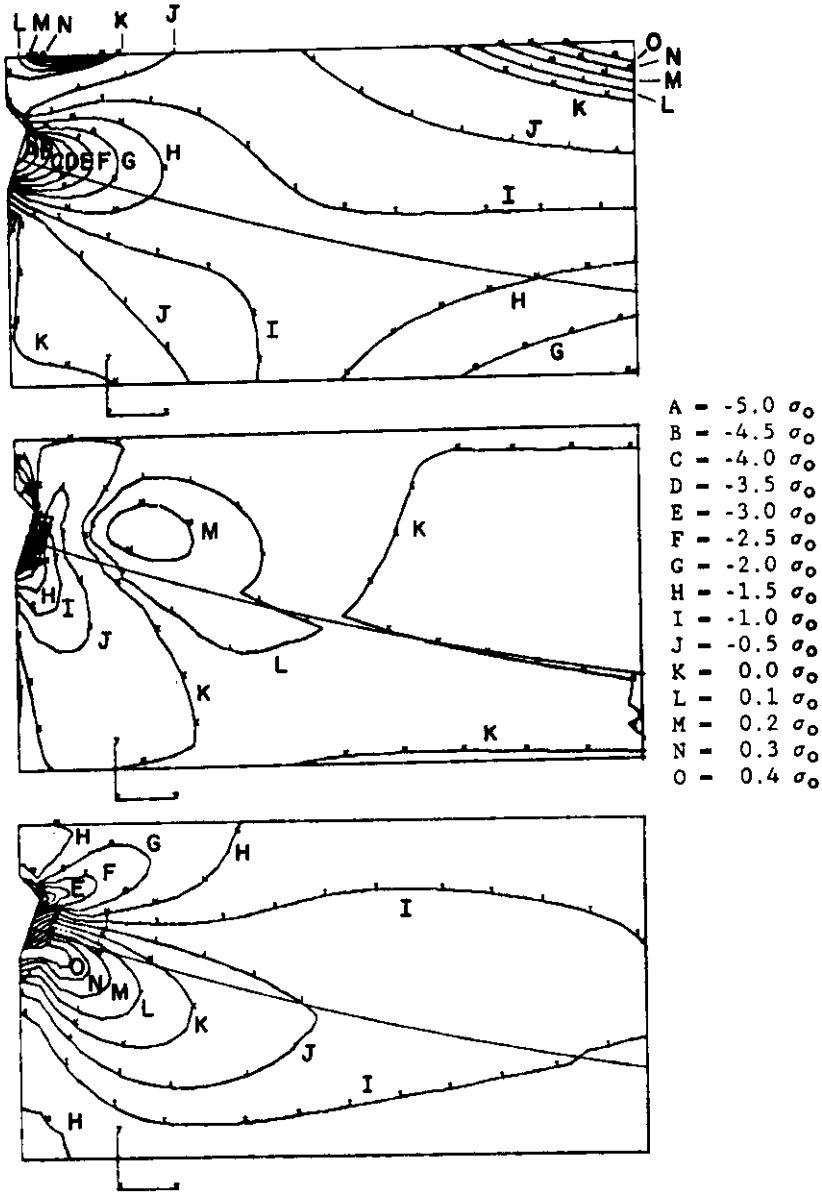

Figure 49. Contour plot of the normal stresses σ_{xx} and σ_{yy}, and of the shearing stress τ_{xy} in an anchorage zone.

developed at the turn of this century, it is still a powerful concept and is the basis for the code provisions for shear design in many countries (Figure 52). Schlaich, et al. (2) proposed to generalize the truss model and to use it in the form of strut-and-tie models for the design of the disturbed regions of a structure in the vicinity of static or geometric discontinuities.

In strut-and-tie models the flow of forces in a structure is approximated by a two-force member system formed of compression members, the struts, tension members, the ties and nodes where the members intersect. The forces in the members are determined from equilibrium conditions, and can then be used to evaluate compressive stresses in the concrete and to proportion the reinforcement. Besides being an approximation to the state of stress in a structure, the strut-and-tie model can also be interpreted as a lower bound solution to a plastic limit load in the context of theory of plasticity.

Schlaich proposes to divide a structure into B-regions and D-regions (2). In B-regions *beam* theory applies and traditional design and analysis methods may be used. D-regions are the *disturbed* regions in the vicinity of static or geometric discontinuities. The extent of these D-regions may be estimated using the principle of Saint Venant (Figure 5). The forces acting on a D-region are the external loads and the internal forces at the boundaries between the D-region and adjacent B-regions. The internal forces can be determined from flexural theory.

In a next step the flow of forces in the D-region is approximated by a series of compression struts and tension ties that are connected at nodes. This strut-and-tie model must establish a load

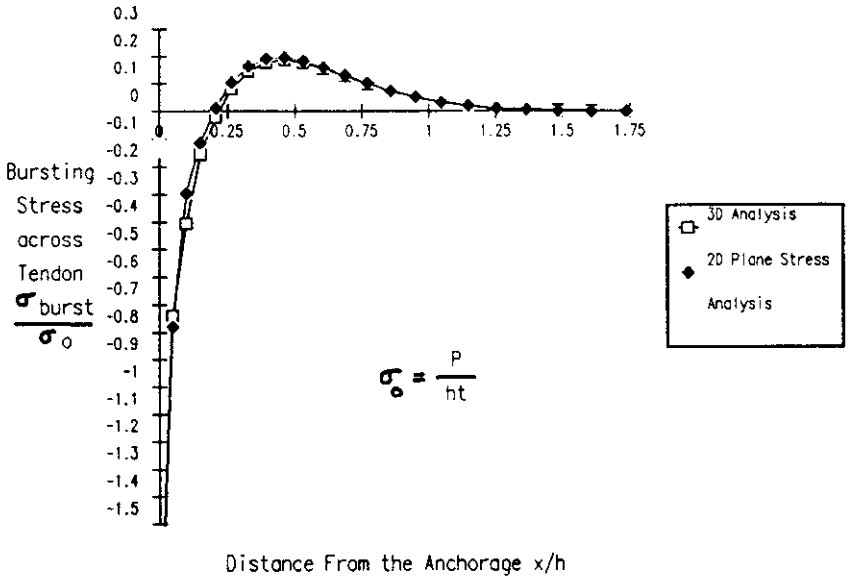

Figure 50. X-Y plot of the stresses perpendicular to the axis of the tendon σ_{xx} represented along the axis.

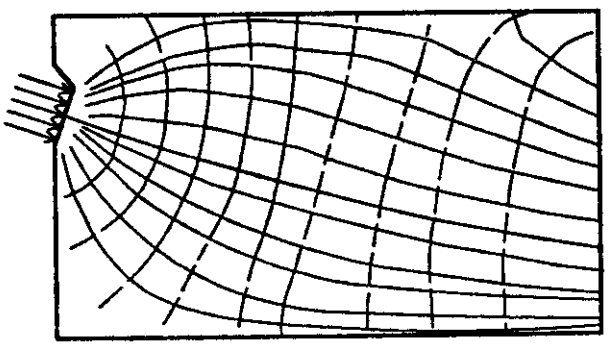

a) Isostatic Lines

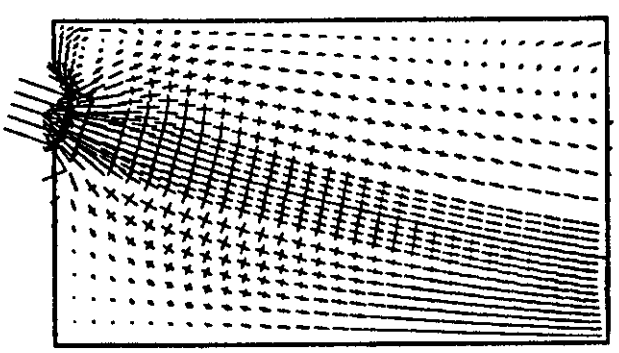

b) Principal Stress Vectors

Figure 51. Isostatic lines and principal stress vectors in an anchorage zone.

path between the external and internal loads acting on the D-region, and must satisfy equilibrium conditions. The ties represent the reinforcement in the structure. The struts represent compression stress fields.

Finally, reinforcement is proportioned based on the tie forces obtained from the strut-and-tie model. Compressive stresses may be checked by assigning a width to the struts. The strut widths are controlled by the dimensions of bearing plates, the dimensions of the overall D-region, and the reinforcement arrangement.

Figure 53 shows a strut-and-tie model for an eccentrically loaded anchorage zone. Reinforcement is visualized as being anchored through bearing plates. The strut widths were selected such that all struts are stressed equally. This causes a hydrostatic state of stress in the nodes and is characterized by the node boundaries perpendicular to the struts. A nonhydrostatic state of stress in the nodes is acceptable if the ratio of stresses on adjacent edges of a node is not less than 0.5 or no more than two (*2*).

The state of stress in the struts is assumed as uniaxial and uniform over the strut width. The stresses are critical at nodal points where bottle necks in the compression fields occur. Schlaich recommends the following values for the nominal concrete strength, $f_c = v_e f_c'$, for struts: $v_e = 0.85 f_c'$ for an undisturbed uniaxial state of stress; $v_e = 0.68 f_c'$ if moderate cracking parallel to the strut may occur or in regions where reinforcement is anchored; $v_e = 0.51 f_c'$ for skew cracking or skew reinforcement; and $v_e = 0.34 f_c'$ for skew cracking with large crack widths.

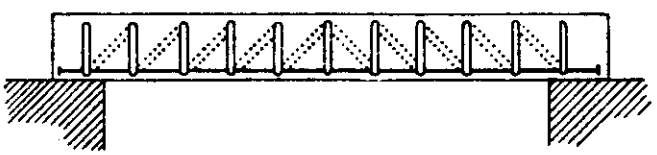

Figure 52. Ritter's truss model.

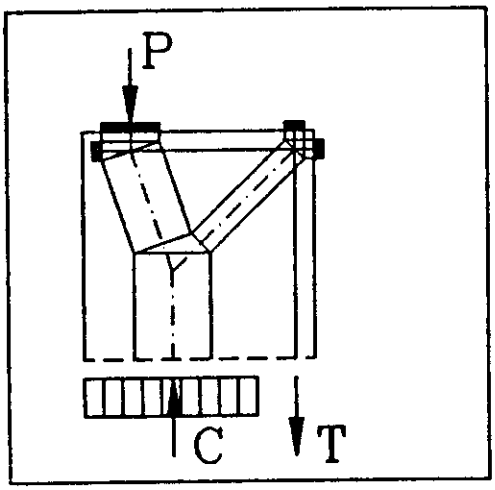

Figure 53. Strut-and-tie model for eccentrically loaded anchorage zone.

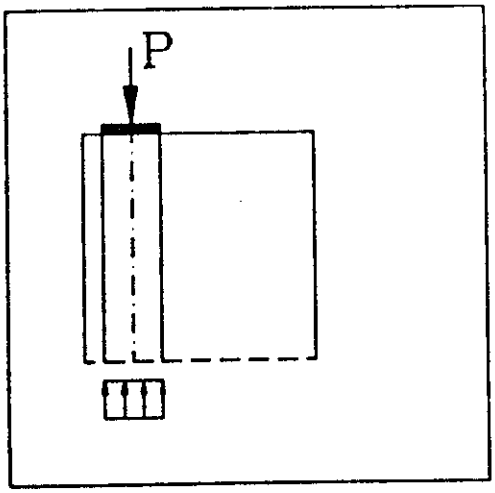

Figure 54. Direct load path in eccentrically loaded anchorage zone.

There is no unique strut-and-tie model solution for a given problem. Rather, any strut-and-tie model that satisfies equilibrium and for which the effective concrete strength and the yield strength of the reinforcement are nowhere exceeded is a lower bound to the plastic limit load. Figure 54 shows an alternative load path for the eccentrically loaded anchorage zone discussed above. This model consists of a single strut that connects the applied load to a uniform stress distribution that extends only over a portion of the end of the anchorage zone. This is a perfectly acceptable lower bound solution, provided the concrete stresses in the strut do not exceed the effective concrete strength. However, this load path does not provide much guidance as to the reinforcement requirements and should not be used.

This example illustrates that equilibrium conditions and material strength limitations alone are not sufficient to develop reasonable strut-and-tie models. Additional rules are needed to eliminate unsatisfactory solutions. The most important rule was already discussed—the internal forces at the boundaries of the D-region should be determined from flexural theory. This requirement provides substantial additional information for the development of a strut-and-tie model, as can be seen by comparing Figure 54 to Figure 53. The enforcement of a flexural theory stress distribution is equivalent to reintroducing compatibility conditions along the interface of the D-region and the adjacent B-region.

There is still considerable freedom in the selection of the strut-and-tie model geometry, even with the restriction discussed above. Schlaich, et al., recommend the orientation of the strut-and-tie model according to the elastic stress trajectories with deviations up to 15 deg. as acceptable (*2*). But even if results of an elastic stress analysis are not available, the flow of the stress trajectories generally can be estimated using engineering judgment with sufficient accuracy for the development of a strut-and-tie model (Figure 45).

Obviously, the approximation of the state of stress in a structure by strut-and-tie models is highly idealized. Such models, therefore, are not particularly useful as research models, where usually more accurate predictions are desired. However, strut-and-tie models are an excellent tool for ultimate load design. The designer is led to visualize a clear load path in the structure and attention is directed to global equilibrium. Furthermore, tie forces can be translated directly into reinforcement requirements and the importance of well-anchored reinforcement is emphasized by the nodal concept.

Strut-and-tie models have only a limited capability to detect compatibility and constraint induced stresses. However, such stresses disappear upon cracking of the concrete and reinforcement is required for crack control, but not for structural safety. This is well established for the case of compatibility torsion, for example. Consequently, crack control reinforcement should supplement the primary reinforcement determined from a strut-and-tie model. The regions where such crack control reinforcement are required can be determined from linear elastic analysis, experience, and common sense. As long as adequate reinforcement is provided for the primary load path, the amount of supplementary crack control reinforcement is not critical in terms of ultimate capacity.

For the designer inexperienced in the use of strut-and-tie models, most likely the biggest problem is the nonuniqueness of the solution. In fact, to a certain degree, a reinforced concrete structure can and will adjust to the load path envisioned by the designer. This adjustment does not even require a perfectly plastic material, but is induced by the change of stiffness and by the stress redistributions that come with cracking of the concrete.

Verification of Strut-and-Tie Models

Part of this project was an experimental study to evaluate the use of strut-and-tie models as a tool for the design of the general zone (*1*). Sanders conducted 36 tests of general anchorage zone specimens. Results will be reported later in this chapter. In the tests the local zone was adequately confined to preclude failure in this region. Tendon configurations included concentric, eccentric, multiple, and curved and inclined tendons. Other variables were reinforcement distribution, presence of lateral post-tensioning, and concrete strength. All specimens had a rectangular cross section except one which had a T-section.